T H E U N I V E R S I T Y O F M I C H I G A N

COLLEGE OF ENGINEERING
Department of Aeronautical and Astronautical Engineering
High Altitude Engineering Laboratory

Scientific Report

UPPER AIR NEUTRAL COMPOSITION MEASUREMENTS BY MASS SPECTROMETER

E. J. Schaefer
M. H. Nichols

ORA Project 05627

under contract with:

NATIONAL AERONAUTICS AND SPACE ADMINISTRATION
CONTRACT NO. NASr-54(05)
WASHINGTON, D.C.

administered through:

OFFICE OF RESEARCH ADMINISTRATION ANN ARBOR

January 1964

TABLE OF CONTENTS

LIST OF TABLES

LIST OF FIGURES

Figure

Upper Air Neutral Composition Measurements by Mass Spectrometer

Edward J. Schaefer and Myron H. Nichols[1]
Department of Aeronautical and Astronautical Engineering
The University of Michigan, Ann Arbor, Michigan

Abstract

A quadrupole mass spectrometer has been designed for studies of neutral atmospheric composition between 100 and 200 km using a Nike-Cajun rocket. A successful technique of ejecting the payload at altitude from an evacuated volume to reduce contaminants has been developed. The ion source has been designed for direct immersion in the ambient atmosphere with the greatest open-look angle possible. The number of surface collisions experienced by a particle prior to ionization has thereby been reduced to the order of one or two and the probability of surface recombination of atomic oxygen has been correspondingly reduced to the order of 1%.

The first successful flight of a continuing program yielded an O_1/O_2 current ratio which was unity at 118 km and 3.1 at 134 km. These values are about an order of magnitude greater than those obtained heretofore by other investigators and achieve much closer agreement with ultra-violet measurements, and theoretical predictions.

On the basis of the data obtained from this flight, a mean molecular weight of approximately 25.3 is derived at 134.5 km.

INTRODUCTION

In the latter part of 1958, a research group at The University of Michigan undertook to develop an instrumentation for measuring the ambient neutral composition. The chief objective was to design a mass spectrometer which would reduce the probability of surface recombination of atomic oxygen to a negligible value. In this manner, it was anticipated that flight measurements of atomic oxygen would be in closer agreement with theory [Nicolet, 1960] and with values obtained from ultra-violet absorption measurements [Byram et al., 1955] than have been obtained by earlier mass spectrometer measurements [Meadows and Townsend, 1960; Pokhunkov, 1962]. In addition, techniques to achieve negligible errors due to chemical reactions at the filament and out-gassing of the rocket were to be developed.

A further objective was to design the experiment for use aboard a small vehicle such as the Nike-Cajun so that a time and latitude survey would be ultimately possible.

A successful flight test of the instrumentation was accomplished on 18 May 1962. The observed O_1/O_2 current ratios were approximately an order of magnitude greater than those obtained by former mass spectrometer measurements [Schaefer, 1963]. This paper gives a detailed description of the instrumentation and techniques employed in making these measurements. Experimental results are presented in detail.

1. INSTRUMENTATION

After a review of the types of mass spectrometers and ion sources suit-

able for the mass number range 4 to 46 and adaptable for use on small rockets, the massenfilter first described by Paul et al. [1958] was chosen. Figure 1 is a line schematic of the mass spectrometer. Ambient neutral particles which enter the volume enclosed by grid G are subjected to electron bombardment. The maximum velocity of the positive ions thus formed is determined by the potential of grid G which serves the dual function of accelerating the ionizing electrons from filament F and providing the electric field gradient to accelerate the positive ions toward the ground plane C and inlet port I. The ions which emerge from the inlet port are subjected to transverse electric fields created by the combined RF and DC potentials applied to the four analyzer rods R. The mass-charge ratio of the ions which reach the collector K is controlled by the rod potentials. Other ions are removed because of their instability in the transverse electric fields which causes them to gain transverse components of motion of sufficient magnitude to result in a collision with a rod. The collector current yields a mass spectrogram with a mass scale having linear dependence on the rod potentials which are swept from zero to peak value linearly with time. The theory of operation of the analyzing section is described by Paul et al. [1958] and a complete description of the spectrometer as adapted for rocket use is given in Schaefer and Nichols [1961]. Table 1 gives the major design parameters of the flight instrument and a photograph appears in Figure 2.

The grid G is operated between 45 and 50 V which, in conjunction with the design parameters of Table 1, provides a resolution of 19 for nitrogen (amu 28) where the peak width is measured at 5% of the peak height.

As is evident from Figures 1 and 2, the ion source is directly exposed to the ambient atmosphere, there being no inlet tubes or enclosing walls. The design of the "open" ion source is made possible by a property of the Paul spectrometer by which the indicated ion mass is independent of the axial ion velocity in the analyzer. Only the percentage transmission and the resolution are dependent on ion velocity.

The total area, 1.3 cm^2, of the analyzing chamber breather holes H (Figure 1) as compared with the area of the inlet port I, 5.1×10^{-3} cm^2, insures that only a negligible fraction of the gas in the analyzer is returned to the ion source. This, together with the open ion source, guarantees that each ambient atom or molecule experiences, on the average, the order of one surface collision prior to ionization. After ionization, a collision with any surface will result in loss of the ion. An attendant feature of the ion source is essentially zero time constant in reaching equilibrium with the environment.

In order to eliminate contamination from a mixture of gases trapped in the rocket and adsorbed on its surfaces, the entire instrumentation is enclosed in a sealed capsule which is ejected from a container when altitude is reached. Prior to launch, the container is evacuated and then back-filled with helium to one atmosphere of pressure. A pop-out diaphragm permits release of the helium on the upleg portion of the trajectory prior to ejection. It may be of interest to note that the capsule is always in the vicinity of room temperature (300°K), because it is separated from the rocket parts heated by aerodynamic effects prior to initiation of data analysis.

During flight, the mass spectrometer is operated in two alternate modes [Schaefer and Nichols, 1961]. In one mode, only one narrow band of mass-charge ratios can reach the collector at any rod excitation potential. The collector output yields the conventional mass spectrogram consisting of a series of peaks, the positions of which determine the mass-charge ratios of the ion species and the amplitudes of which indicate the abundances. In the other mode, all ions are stable at low rod voltages and reach the collector. As the rod voltages are increased, ions are removed, one species at a time, in order of increasing mass-charge ratios. The collector output is a series of steps. This mode of operation and its spectrogram are called "staircase." The two modes are illustrated in Figure 5. From Figure 2 of Schaefer and Nichols [1961] (and checked by Figure 5), it is evident that the mass number scale for the peak spectrum must be multiplied by approximately 9/7 to give the mass number scale of the staircase mode. Both modes are useful in interpreting the data. For example, the staircase mode gives the total residual ion current due to ions whose masses lie above the mass range of the instrument. When approaching the sensitivity limit of the instrument where the mass peaks tend to be lost "in the noise" their presence is revealed by the staircase mode and a more precise result can be obtained. At increasingly high pressures sensitivity reaches a maximum then decreases due to scattering collisions and the staircase degenerates into a curve rather than a series of steps whereas the spectral peaks show no significant change in shape. Thus the staircase mode identifies the branch of the double-valued curve upon which the instrument is operating. Finally, the staircase mode

assures 100% transmission and therefore serves as a calibration of the major peaks.

Prior to flight, laboratory calibrations were run on the entire instrumentation using air. A high speed vacuum system was used in connection with an adjustable leak in order to minimize the effect of adsorption on the walls of the system and interaction with the hot filament electron source until the ultimate vacuum was approached. Figures 3 and 4 serve to illustrate the results of preflight laboratory calibrations which were made by first increasing the pressure from the ultimate and then decreasing the pressure. The fork in the O_2/N_2 current ratio at low pressures (Figure 3) is probably due to the greater affinity of O_2 for the chamber walls which operates to deplete it on the increasing pressure cycle and enrich it due to desorption on the decreasing pressure cycle.[2] In the reduction of flight data to obtain number densities, a linear response of the instrument to O_2 density below 10^{-5} mm Hg total pressure was assumed. The apparent enrichment of argon at low pressures (Figure 4) as evidenced by the A/N_2 current ratio may be due to the nature of the leak or the characteristics of the pump. Both O_2 and A show apparent enrichment at higher pressures due to scattering collisions and their smaller cross sections as compared with N_2. In both cases it will be noted the staircase yields the more accurate ratio at high pressures because of the stronger focusing action in this mode of operation.

As evident in Figure 3, these preflight calibrations yielded an O_1/O_2 current ratio of about 0.04. This result indicates that the average electron energy was less than 45 V due to space charge effects around the fine wires of the accelerating grid. The basis for this conclusion is given in Section 3. The N_1/N_2 current ratio was about 0.015.

2. FLIGHT DATA

The instrumentation described in the previous section was flown on Nike-Cajun rocket NASA 10.91 UA from Wallops Island, Va. (latitude 37°50'N, longitude 75°29'W) at 1302 EST, May 18, 1962. Apogee was 134.5 km and the horizontal velocity at apogee was approximately 0.24 km/sec. The spin period was 1.2 sec and the precession period was 31 sec.

To provide the reader with some feeling for the quality of the data, Figure 5 is a photograph of unretouched telemetered conventional and staircase spectra at 120 km altitude upleg. Figures 6a, b, c, d and e show raw, uncorrected ion current as a function of altitude for total current, N_2, O_2, O_1 and A. Figures 7a, b and c show the number densities in the ion source for N_2, O_2 and A as obtained from the raw data by means of laboratory calibrations.[3]

Figure 8 shows the ratio of O_1 ion current to O_2 ion current. The interpretation of this ratio in terms of number densities requires a knowledge of the relative ionization cross sections of O_1 and O_2. The results for the minor constituents are given in Appendix A.

3. CORRECTION FOR RELATIVE IONIZATION CROSS-SECTIONS FOR O_1 AND O_2

Since no means for generating neutral O_1 atoms were available to us for laboratory calibration, it is necessary to use published data on the O_1 ionization cross section. Also, as already mentioned, we are uncertain as to the effective energy of the ionizing electrons because of space charge effects in the neighborhood of the fine wires constituting the electron accelerating grid.

Data on the ionization cross-sections of O_2 and O_1 [Fite and Brackmann, 1959] indicate that, for 45 eV, the relative O_1/O_2 cross-section ratio is approximately 0.85. However, since our laboratory calibrations showed 4% O_1 ions, the data of Fite and Brackmann indicate that the effective energy was

in the neighborhood of 25-30 eV. At this energy, their experimental data also indicates that the ratio of the O_1 cross-section to the O_2 cross-section is nearly unity although the theory indicates a ratio of approximately 0.5. In the data interpretation in this paper, an ionization cross-section ratio of unity will be assumed. Under this assumption, Figure 8 also gives the ratio of number densities of O_1 to O_2 in the ion source.

4. INTERPRETATION OF THE DATA—DYNAMIC EFFECTS

It is the purpose of this section to discuss effects of dynamics on the interpretation of the results. Precise quantitative analysis is prohibitively complicated in view of the involved geometry of the ion source, the varying (and on this flight not precisely known) angle-of-attack and the nature of the interactions between the impinging atoms and molecules and the atoms of the base metal with an adsorbed gas layer.[4]

In the altitude range of interest, the mean free path is much larger than the dimensions of the apparatus, so the condition for free molecular flow is satisfied. Because of the low ambient densities necessary for free molecular flow conditions and the difficulty of determining surface conditions, obtaining valid laboratory data on surface interactions presents experimental difficulties [Hartnett,1961]. Consequently, few data are available. Results of Smith and Fite [1963] show diffuse and specular reflection in various degrees depending on surface conditions, surface temperature and on the temperature of the beam. For argon on nickel, when the target temperature is the same or higher than the kinetic temperature of the beam, the scattering from the surface tends to be diffuse whereas when the beam temper-

ature is much higher than the target temperature, the scattering tends toward specular in that the angular position of the intensity peak of the reflected particles approaches the angle of incidence. The results of H_2 on nickel are much more complicated.

In view of the above remarks, it is possible to establish only rough bounds on the effects of interaction with the metal surface.[5] In the following, two models are considered, in each case neglecting recombination effects.

A. Perfect reflection model. In this model it is assumed that the normal component of the particle velocity is reversed upon collision with the surface and that the velocity of the body is normal to the surface. The number density $n_{i_{eff}}$ of the ith species just outside the surface, which represents the number density in the ion source, is

$$n_{i_{eff}} = \frac{2n_i}{\sqrt{2\pi}} \int_{-\infty}^{x_i} \exp(-t^2/2)dt \qquad (1)$$

where $x_i = V(m_i/kT)^{1/2}$

T = ambient temperature in °K

n_i = ambient number density of the ith species, particles/c.c.

V = velocity of the body, cm/sec.

m_i = particle mass of ith species, gms.

k = Boltzmann's constant = 1.38×10^{-16} erg deg^{-1} K

Thus at zero velocity, the presence of the surface has no effect whereas when $x_i \gg 1$ the effect of the surface is to double the ambient density. This model gives the lower bound of the interaction effects.

B. Complete thermalization model. In this model, it is assumed that the impinging particles reach complete thermal equilibrium with the surface and are subsequently reemitted, retaining the temperature of the surface. The number density just outside the surface is obtained by requiring that the rate of arrival of particles of the ith species is the same as the rate of departure. The total number density $n_{i_{eff}}$ of the ith species is

$$n_{i_{eff}} = \frac{n_i}{\sqrt{2\pi}} \int_{-\infty}^{x_i} \exp(-t^2/2)dt + \frac{n_i}{2} \left(\frac{2\pi m_i}{kT_s}\right)^{1/2} \left\{ \left(\frac{kT}{2\pi m_i}\right)^{1/2} \exp(-x_i^2/2) + \frac{V}{\sqrt{2\pi}} \int_{-\infty}^{x_i} \exp(-t^2/2)dt \right\} \quad (2)$$

where the symbols are the same as above and

T_s = temperature of the surface in °K.

For zero velocity this gives the same result as perfect reflection if the ambient temperature and the surface temperature are equal—i.e., if $T = T_s$. For very large velocities, such that $V \gg (kT/m_i)^{1/2}$,

$$n_{i_{eff}} \rightarrow \frac{n_i}{2} \left(\frac{2\pi m_i}{kT_s}\right)^{1/2} V \quad . \quad (3)$$

Thus for large V, the effective density can be a large factor times the ambient density. Also at large V, the effective density is increased in proportion to $m_i^{1/2}$.

Since a number of collisions is required to approach complete thermalization, it is apparent that this model gives an upper bound to the surface interaction effect.[6]

Figure 9 is a comparison of the two models in terms of the enrichment

of O_2 over O_1 due to the surface interaction effects. Recombination of O_1 is neglected and a surface temperature of 300°K is assumed. To give some feeling for the effects of ambient temperature on the enrichment factor, two sets of curves, computed on the basis of assumed ambient temperatures of 200°K and 500°K, are presented. These temperatures are representative of the extremes encountered in the altitude range of interest. Based on the previous discussion, there is reason to suspect that at high velocities the true effect lies closer to the perfect reflection model than to the complete thermalization model.

From the ion current data (Figure 6a) it is clear that the minima in the up and down curves are all spaced closely to 31 sec apart. This can be explained by precession as indicated schematically in Figure 10. The precession cone half-angle is estimated in Appendix C to be 44°. The higher O_1/O_2 ratios which occur in the minima of ion current on the downleg as seen in Figure 8 can be explained by the higher thermal velocity of O_1 relative to O_2. This enables relatively more O_1 atoms than O_2 molecules to reach the ionizing region in the ion source at angles of attack greater than 90°.

In interpreting the data it is important to note that the minima of the upleg data at 108 km, 123 km, and 133 km, approximately, and the maxima of the downleg data at 127 km and 111 km fall closely to a single smooth curve. On the basis of Figure 10, this may be explained by the hypothesis that the instrumentation is flying more closely to right angles to the trajectory at these points. From Figures 1 and 2 it is evident that for particles enter-

ing the ion source, the least interaction occurs for angles of attack near 90°. On this basis, it may be postulated that the data most closely relate to ambient conditions at these points.

It is also important to note from Figure 8 that between 108 km and 117 km and also in the neighborhood of 128 km (above which there is sufficient spread in the data to obscure the effect) the O_1/O_2 upleg ion current ratios are nearly identical to the downleg. Based on Figure 10, the authors roughly estimate the angle of attack at 108 km on the upleg at about 55° and at 113 km on the downleg at about 105°. Since these angles are quite different and yet the upleg and downleg O_1/O_2 ion current ratios in this range of altitudes are nearly the same, one is led to the hypothesis that the interaction with the metal surfaces is closer to perfect reflection than thermalization. However, it should be pointed out that the rather large ring at the top of the ion source, which can be seen clearly in Figure 2, can interact with the gas flow, that the precession cone half-angle of 44° is only approximate, and that we have no direct knowledge of the attitude of the instrumentation during the flight. In future flights, the surface area of the ring will be substantially reduced.

5. MEAN MOLECULAR WEIGHT

In order to minimize surface interaction effects in computing the mean molecular weight, the data at the minima in the upleg and at the maxima in the downleg are used. These are tabulated in Table 2, in terms of number density in the ion source. The number density for O_1 in the ion source is obtained from the number density of O_2 in the ion source multiplied by the O_1/O_2 ion current ratio (Figure 8) assuming no surface recombination (Appen-

dix B) and equal ionization cross sections as stated in Section 3.

The mean molecular weight at any altitude is given by

$$M = \frac{\sum_{i=1}^{k} n_i M_i}{\sum_{i=1}^{k} n_i} \qquad (4)$$

where n_i is the ambient number density of the ith component and M_i is its molecular weight. The number densities in Table 2 are the number densities in the ion source taken at the points in the trajectory where, as previously discussed, it is evident that the least amount of surface interaction occurs. If no correction for surface interaction is applied, the points plotted as crosses in Figure 11 result. In order to illustrate surface interaction effects, points for the perfect reflection model and the complete thermalization model are also plotted. If Equation 1 for perfect reflection is used plus a correction for recombination of O_1, the points plotted as circles result. The recombination correction assumes one collision on the average and a probability of recombination of 0.01 per collision (see Appendix B). If Equation 2 for complete thermalization plus the same recombination correction are used, the points plotted as triangles result.[7] Based on the previous discussions, it appears to be most likely that the true values lie closer to the crosses and circles than to the triangles. The solid curve of Figure 11, arbitrarily drawn on this basis, indicates the authors' best estimate of the true value of mean molecular weight.

It is interesting to note that the value of 24.4 for the mean molecular

weight given in the 1956 ARDC model atmosphere at 135 km is in much better agreement with our data than the value of 28.5 at the same altitude in the 1959 ARDC model atmosphere.

6. COMPARISON OF RESULTS

A. Dissociation of oxygen. Figure 12 compares our results with those of Meadows and Townsend [1960] and Pokhunkov [1960]. The results of Meadows and Townsend [1960] were taken from the data of Aerobee-Hi NN 3.19F fired from Fort Churchill, Manitoba, Canada, at 1207 CST on March 23, 1958. Although their paper does not present a plot of the O_1/O_2 current ratio, the curve in Figure 12 was obtained by dividing the values of the O_1 currents by the O_2 currents contained therein. As discussed in Section 1 and Appendix B, the lower ratio obtained by the other investigators may be attributed to surface recombination in the apparatus.

B. O_2 number densities. Figure 13 compares our results with those of Byram et al. [1955] and of Hinteregger [1962]. In this figure our data are uncorrected for dynamic effects. To provide some feeling for the magnitude of the surface interaction effects, Table 3 gives the computed factors by which the O_2 density in the ion source exceeds the ambient density for the perfect reflection model and the complete thermalization model discussed in Section 4. The plane surface has been assumed normal to the direction of motion and the ambient and surface temperatures have been assumed equal to 300°K.

It should be noted that in our case the ion source in not an ideal plane and, from Figures 7b and 10, it is evident that the angle of attack

is continually changing.

C. Separation ratio of argon and nitrogen. Figure 14 compares our results with those of Meadows-Reed and Smith [1962] in terms of a separation ratio, r, defined as ion current ratio at altitude[8] divided by the current ratio from ground air calibration. Points from the results of sampling techniques by Wenzel et al. [1960] and Mirtov [1957] are included. For reference purposes, the dotted curve is the separation ratio computed for isothermal diffusive equilibrium taken from Figure 6 of Meadows and Townsend [1960].

Figure 15 compares our results with those of Pokhunkov [1963a] on the basis of A/N_2 current ratios at altitude.

At this time we have no detailed quantitative explanation for the difference in the character of our results and those of Meadows-Reed and Smith and Pokhunkov. (We note that the time constant of our ion source in reaching equilibrium with the ambient atmosphere is essentially zero.) However, our results are not inconsistent with those obtained by sampling techniques (Figure 14).

ACKNOWLEDGMENTS

The research described herein has been supported by the National Aeronautics and Space Administration under contracts NASw-138 and NASr-54(05).

The authors are indebted to L. M. Jones for his encouragement and assistance throughout the program. Others who made this paper possible are N. J. Wenk and W. H. Hansen for the mechanical designs, C. H. Thornton and E. A. Wenzel for the electronic circuitry and H. F. Henry for the construction of the ion sources. The authors are indebted to J. Brown for his assistance in preparing the figures for this paper as well as his many contributions in research. Many helpful discussions with P. Hays are gratefully acknowledged. M. Dubin and (Mrs.) E. B. Meadows-Reed of the NASA have provided many stimulating discussions in the field of upper atmosphere research.

APPENDICES

A. MINOR CONSTITUENTS

Throughout this section, the reader is cautioned that peak-peak noise on the telemeter channel was equivalent to 3×10^{-12} A, approximately, at the electrometer input. Comments made throughout this section must therefore be regarded as tentative inasmuch as most of these constituents reach the noise level prior to apogee.

A.1. ATOMIC NITROGEN

Atomic nitrogen was apparent in both the conventional spectra and staircase spectra. The average value between 100 km and apogee lay between 0.02 and 0.04 of the N_2 ion current. Unfortunately, because of noise and resolution limitations no firm conclusions can be drawn from the results of this flight regarding possible dissociation of nitrogen except that N_1 probably exists at no greater concentration than 0.05 N_2. This is particularly true since the laboratory calibration data yielded a ratio of N_1/N_2 of 0.015, somewhat less than observed in flight, but not conclusive in the presence of noise.

A.2. WATER

Figure 16 shows the raw data points obtained from both staircase and conventional spectra for the mass 18 peak. The wide divergence between the staircase data and spectral peak data is probably due to the large kinetic cross section of the water molecule. Here, again, the staircase mode yields the larger values due to the strong focusing action which overcomes

the effects of scattering collisions to higher densities than the conventional mode of operation. Since upleg and downleg data show many of the characteristics of the major constituents, the authors suspect that a substantial portion of the current was due to the ambient atmosphere. It appears likely that the rising currents with decreasing altitudes on the downleg, for example, cannot be explained on the basis of out-gassing of the ion source alone.[9] However, data from future flights will be awaited before further work on this constituent will be undertaken.

A.3. MASS 44 AND RESIDUAL ION CURRENTS

The mass 44 spectral peak current is shown as a function of altitude in Figure 17. This peak may be due to CO_2 or N_2O both of which have a mass of 44 amu. The rf voltage at the end of the sweep was large enough to clearly show the mass 40 step in the staircase mode but was not sufficient to include the mass 44 step. Hence, the residual current (Figure 18) obtained from the staircase mode, includes the mass 44 ion current together with all constituents greater than mass 40.

Unfortunately, the mass 44 peak was too small to detect in the presence of noise except at the lower part of the trajectory. In the altitude range for which it is shown (Figure 17) it exhibits many of the characteristics of the major constituents. This suggests that a significant portion of the mass 44 peak is of ambient origin.

On the other hand, if one were to subtract the mass 44 ion current from the residual current of Figure 18, the remainder would be almost constant with altitude. This leads to the conclusion that the residual components

above mass 44 are almost entirely due to constituents which emanated from the metal surfaces in the vicinity of the ion source.

B. RECOMBINATION EFFECTS IN EARLIER MEASUREMENTS

Earlier measurements of O_1/O_2 were made using Bennett tubes. The typical Bennett tube has many grids so that after an oxygen atom has entered the tube it may be expected to have many collisions with grids and walls before it finds its way back out. Although the grids are relatively transparent when viewed along the axis they become less so at angles relative to the axis, approaching opaqueness at 90°. Thus the grids have a sort of trapping effect which, among other things, can result in numerous passages in the ionizing region. This results in an increased probability of ionization of the trapped components relative to the incoming atom or molecule, which must be partially collimated in order to reach the ionizing region before interacting with the walls.[10] Assuming that the difference between our results and the earlier results is due to recombination in the apparatus, the following is an attempt to provide some insight into the phenomenon.

A detailed analysis of a particular tube would be prohibitively complicated. However, some feel for the situation may be achieved by use of a simplified two-dimensional model. Let the Bennett tube be replaced by a cylinder with its axis in the x direction and consider motion in a plane including the x axis. Let the distance between the walls be unity. Let the angle of scattering from the walls be θ measured from the normal. Assume that the angle of scattering is independent of the angle of incidence. Let

the probability density function of θ be

$$p(\theta) = (2/\pi) \cos^2\theta \qquad -90° < \theta < 90° \tag{5}$$

This function is rather mildly peaked at $\theta = 0$ to represent preponderance of scattering normal to the axis of the tube due to the grids, etc. The distance traveled along the axis of the cylinder between collisions with the walls is given by $\tan \theta$. From (5) the distribution function of $\tan \theta$ is

$$p(\tan \theta) = (2/\pi) \cos^4\theta = 2/\pi(1+x^2)^2 \tag{6}$$

where $x = \tan \theta$. The rms value, σ_x, of x is

$$\sigma_x = 1 \quad . \tag{7}$$

After N bounces, the mean of the sum of the individual x's is zero and the rms value σ_{Nx} is

$$\sigma_{Nx} = \sqrt{N} \quad . \tag{8}$$

If N is large, then it may be assumed that the distribution of the sum is approximately Gaussian. If N is 100, for example, then $\sigma_{Nx} = 10$. Then, assuming a Gaussian distribution, the probability, after 100 wall collisions, of traveling along the x axis a distance of ten diameters or more in one direction is 0.16.

In such a model, an oxygen atom, after entering the ionizing region of the Bennett tube, is very likely to experience many collisions with walls and grids before escaping from the tube. Experimental determinations of

the probability of recombination of atomic oxygen upon collision with a metal under conditions similar to those encountered with a Bennett tube have been reported by Hacker et al. [1961] and by Wood and Wise [1961]. The results may be summarized in Table 4.

For purpose of illustration, Table 5 shows the expected fraction, f_a, of atoms (i.e., fraction not recombined) left after 100 collisions with the surface as a function ρ_c, the probability of recombination per collision.

Thus with the typical Bennett tube, even with a very short inlet tube, it is reasonable to expect very substantial amounts of recombination prior to ionization. With the ion source used in the experiment reported in this paper, an atom can be expected to experience, on the average, only one to two surface collisions prior to its escape.

Wood and Wise [1961] also reported experiments on the recombination of N_1 upon collision with nickel and gold. The probability of recombination on nickel per collision is 0.1 independent of temperatures over the range $1000 > T > 350°K$ and on gold the value is 0.01 at 300°K and 0.1 at 1000°K. Thus one may expect recombination effects to be more severe with atomic nitrogen than with atomic oxygen.

C. ANGLE OF PRECESSION

Assuming that the instrument package is symmetric about the longitudinal axis, the following equation can be used to determine the precession cone half-angle θ (see for example, Slater and Frank [1947])

$$\dot{\phi} \cos \theta = \omega_3 (I_3/I_1) \tag{9}$$

where:

$\dot{\phi}$ = angular velocity of precession

θ = half angle of the precession cone

ω_3 = angular velocity component along longitudinal axis of package.

The received field strength of the telemetry signal shows a period of 1.2 sec which may be associated with ω_3. The ion current data show a period of 31 sec which may be associated with $\dot{\phi}$. The moment of inertia I_3 is about the longitudinal axis of the package and I_1 is the moment of inertia about an axis perpendicular to the longitudinal axis. Both pass through the CG.

The moments of inertia I_3 and I_1 were not measured prior to the flight of NASA 10.91 UA and we have no duplicate package. Therefore, these moments are calculated approximately from our knowledge of the package geometry. Actually, the package was not exactly symmetric. However, assuming that it was symmetric, the calculated ratio I_3/I_1 is 0.028. Substitution into (9) gives

$$\theta = \cos^{-1} 0.72 = 44^\circ \ . \tag{10}$$

Since the ratio of I_3/I_1 is only approximate and may be expected to be subject to error of ± 10% or so, θ may be expected to lie between 40° and 50°. This provides a qualitative explanation of the ion current versus altitude curves.

REFERENCES

Baule, B., Theoretische behandlung der erscheinungen in verduennten gasen, Annalen der Physik, 44, 145-176, 1914.

Byram, E. T., T. A. Chubb, and H. Friedman, Dissociation of oxygen in the upper atmosphere, Phys. Rev., 98, 1594-1597, 1955.

Fite, W. L., and R. T. Brackmann, Ionization of atomic oxygen on electron impact, Phys. Rev., 113, 815-816, 1959.

Gilbey, D. M., A re-examination of thermal accommodation coefficient theory, J. Phys. Chem. Solids, 23, 1453-1461, 1962.

Hacker, D. S., S. A. Marshall, and M. Steinberg, Recombination of atomic oxygen on surfaces, J. Chem. Phys., 35, 1788-1792, 1961.

Hartnett, J. P., A survey of thermal accommodation coefficients, Rarefied Gas Dynamics, pp. 1-28, edited by L. Talbot, Academic Press, New York and London, 1961.

Hinteregger, H. E., Absorption spectrometric analysis of the upper atmosphere in the EUV region, J. Atmos. Sci., 19, 351-368, 1962.

Hurlbut, F. C., Notes on surface interaction and satellite drag, Project Rand, Aerodynamics of the upper atmosphere, R-339, pp. 21-1 to 21-25, compiled by D. J. Masson, 1959.

Istomin, V. G., Mass spectrometric measurements of gas composition of the earth's atmosphere by means of rockets and satellites, Geomagnetism and Aeronomy, 1, 321-328, 1963.

Meadows, E. B., and J. W. Townsend, IGY rocket measurements of arctic atmospheric composition above 100 km, Space Research, pp. 175-198, edited by H. Kallmann-Bijl, North-Holland Publishing Co., Amsterdam, 1960.

Meadows-Reed, E. and C. R. Smith, Mass spectrometric investigation of the atmosphere between 100 and 227 km above Wallops Island, Virginia, NASA Tech. Note TND 1851, 1962.

Mirtov, B. A., Rocket investigation of the composition of the atmosphere at high altitudes, Uspekhi fiz nauk, 43, 181-196, 1957.

Nicolet, M., Physics of the upper atmosphere, pp. 29-35, edited by J. A. Ratcliffe, Academic Press, New York and London, 1960.

Paul, W., H. P. Reinhard, and U. von Zahn, Das elektrische massenfilter als massenspektrometer und isotopentrenner, Zeitschrift für Physik, 152, 143-182, 1958.

Pokhunkov, A. A., The study of upper atmosphere neutral composition at altitudes above 100 km, Space Research, pp. 101-106, edited by H. Kallmann-Bijl, North-Holland Publishing Co., Amsterdam, 1960.

Pokhunkov, A. A., Mass-spectrometer investigations of the structural parameters of the earth's atmosphere at altitudes from 100 to 210 km, Planetary Space Sci., 9, 269-279, 1962.

Pokhunkov, A. A., Gravitational separation, composition and structural parameters of the night atmosphere at altitudes between 100 and 210 km, Planetary Space Sci., 11, 441-449, 1963a.

Pokhunkov, A. A., On the variation in the mean molecular weight of air in the night atmosphere at altitudes of 100 to 200 km from mass spectrometer measurements, Planetary Space Sci., 11, 297-304, 1963b.

Schaaf, S. A. and P. L. Chambre, Flow of rarefied gases, Fundamentals of Gas Dynamics, Sec. H, pp. 687-739, edited by H. W. Emmons, Princeton University Press, 1958.

Schaefer, E. J., The dissociation of oxygen measured by a rocket-borne mass spectrometer, J. Geophys. Res., 68, 1175-1176, 1963.

Schaefer, E. J., and M. H. Nichols, Mass spectrometer for upper air measurements, Am. Rocket Soc. J., 31, 1773-1776, 1961.

Schamberg, R., A new analytic representation of surface interaction for hyperthermal free molecule flow with application to neutral-particle drag estimates of satellites, Project Rand Research Memorandum RM-2313, ASTIA Document No. AD 215301, Jan. 8, 1959.

Slater, J. C., and N. H. Frank, Mechanics, McGraw-Hill Book Co., New York, 1947. (p. 112, Eq. 3.4).

Smith, J. N., Jr., and W. L. Fite, Recent investigations of gas-surface interactions using modulated-atomic-beam techniques, Rarefied Gas Dynamics, Vol. I, pp. 430-453, edited by J. A. Laurmann, Academic Press, New York and London, 1963.

Wenzel, E. A., L. T. Loh, M. H. Nichols and L. M. Jones, The measurement of diffusive separation in the upper atmosphere, Annals of the IGY, Vol. 12, Part 1, pp. 407-421, 1960.

Wood, J., and H. Wise, The interaction of atoms with solid surfaces, Rarefied Gas Dynamics, pp. 51-59, edited by L. Talbot, Academic Press, New York and London, 1961.

LIST OF FOOTNOTES

1. Now at San Diego State College, San Diego, Calif.
2. As part of the mass spectrometer development, calibration curves were run on N_2 and O_2 separately, using the adjustable leak procedure. On the basis of these calibrations, the predicted ratio of O_2 ion current to N_2 ion current for ground air is 0.14.
3. In obtaining these curves, only data above 106 km on the upleg and above 100 km on the downleg were used. Lower altitude data were not used because the density in the analyzing section was high enough to affect the ion currents by scattering collisions as evidenced by a rounded shape of the staircase spectrum. The densities in the analyzing section and ion source could be substantially different in flight because of dynamic effects. Hence, calibration results, obtained at a uniform density in the ion source and in the analyzing section, could be applied only where peak spectral current values are functions of processes in the ion source only.
4. A review of existing theory of surface interactions may be found in Gilbey [1962].
5. A review of surface interaction phenomena with particular reference to the thermal accommodation coefficient has been published by Hartnett [1961]. Reviews relative to the influence of surface interactions on the drag of high speed bodies in the free molecular flow regime have been published by Schamberg [1959], Hurlbut [1959] and Schaaf and

Chambre [1958]. Noting that valid theoretical and experimental data are not available, these authors have made use, for the purpose of estimation, of the results of Baule [1914] which are based on a hard sphere interaction model. To illustrate for the case at hand, using Baule's results with the assumption of one collision with a loosely bound adsorbed layer of O_2, the enrichment factor, E, of Figure 9 is 1.03; assuming two collisions, E becomes 1.04. Using a model similar to that of Baule, but computing a weighted average speed (rather than average energy) over a possibility of one or two collisions with loosely adsorbed O_2, the authors have computed an enrichment factor of 1.1. These values of E are computed for a body velocity sufficiently large that thermal energies of the interacting particles can be neglected. If it is assumed that the interaction is with more massive metallic atoms, the values of E are closer to unity.

6. If trapping of the ambient particles in the mass spectrograph occurs, as discussed in Appendix B, then an approach to thermalization can occur. However, with the open construction of our ion source, such complete thermalization appears to be unlikely.

7. For computing purposes, ambient and surface temperatures of 300°K were used. According to the model atmospheres, this temperature is characteristic of the 110 to 120 km range, with the more recent models giving substantially higher temperatures at 130 km. Also for the computations, the plane surface has been assumed normal to the direction of motion thus giving maximum computed corrections for each model.

LIST OF FOOTNOTES (Concluded)

8. Corrected by Meadows-Reed and Smith for dynamic effects relative to their instrument.

9. Upon admission of a dry gas to an evacuated system, the residual water vapor peak has been observed to increase, probably due to the liberation of water molecules from surfaces under bombardment by the gas molecules. However, for an equivalent change in total pressure, this effect is typically an order of magnitude smaller than the observed change in the water vapor peak which occurred on this flight.

10. In this respect, the authors disagree with Istomin [1963] who assumes that the probability of ionization of the reverse flux is the same as the incident flux. Also, for the same reason, we disagree with the method used by Pokhunkov [1963b] to estimate a correction for his Bennett tube data. (His corrected data for the O_1/N_2 number density ratio agree roughly with ours at 135 km even though his ion current ratio is approximately 1/8 of ours.)

Table 1. Flight Instrument Design Parameters

Length of four-pole field (rod length)	12.75 cm
Field radius (centerline to edge of rod)	0.522 cm
Rod radius	0.609 cm
RF frequency	2.39 Mc
Inlet port diameter	0.081 cm
Maximum ion injection angle	5.25°
Peak RF voltage (for amu 46)	500 V
Spectrum sweep time (sawtooth)	0.5 sec

Table 2. Number Densities in Ion Source

Altitude km	Velocity m/sec	Number Densities in Ion Source in units of 10^{10} per cc			
		O_1	O_2	N_2	A
108 (up)	753	32	72	290	2.5
111 (down)	716	17.4	34.8	152	1.05
123 (up)	530	4.8	2.95	19.0	0.12
127 (down)	452	3.6	1.82	13.0	0.07
133 (up)	301	2.3	0.80	6.4	0.03

Table 3. Dynamic Correction Factors

Altitude	Velocity	Multiplication Factor for O_2	
km	m/sec	Perfect reflection	Complete thermalization
133	301	1.72	2.30
123	530	1.94	3.36
108	753	1.99	4.38

Table 4. O_1 Recombination Probabilities

Metal	Temperature	ρ_c	Authors	Date
Pt	200°C	0.010 ± 0.002	Hacker, Marshall and Steinberg	1961
Pt	850°C	0.10 ± 0.02	Hacker, Marshall and Steinberg	1961
Pt	380°K	0.001	Wood and Wise	1960
Al	364°K	0.017	Wood and Wise	1960
Pt	1100°K	0.004	Wood and Wise	1960

Table 5. Fraction O_1 Remaining After Surface Interaction

ρ_c	f_a
0.01	0.36
0.02	0.13
0.03	0.05

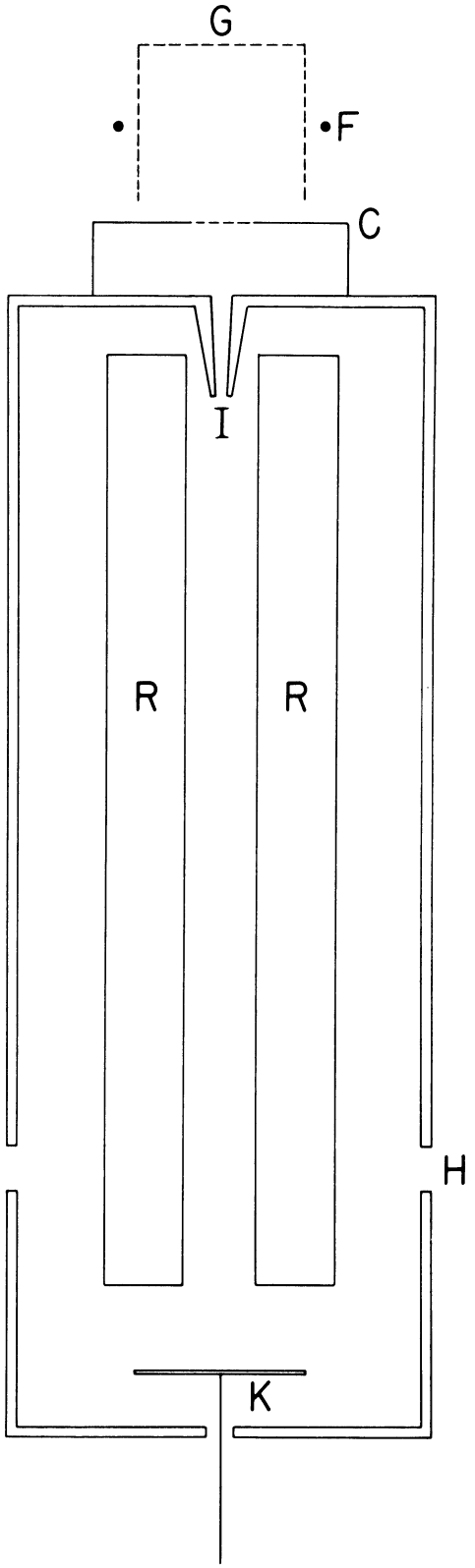

F-FILAMENT, G-ACCELERATING GRID, C-GROUND PLANE
I-ION INLET PORT (DIAMETER=0.081 CM, AREA= 5.1×10^{-3} CM^2)
R-ANALYZER RODS, K-ION COLLECTOR
H-4 BREATHER HOLES (TOTAL AREA=1.3 CM^2)

Figure 1. Mass spectrometer line schematic.

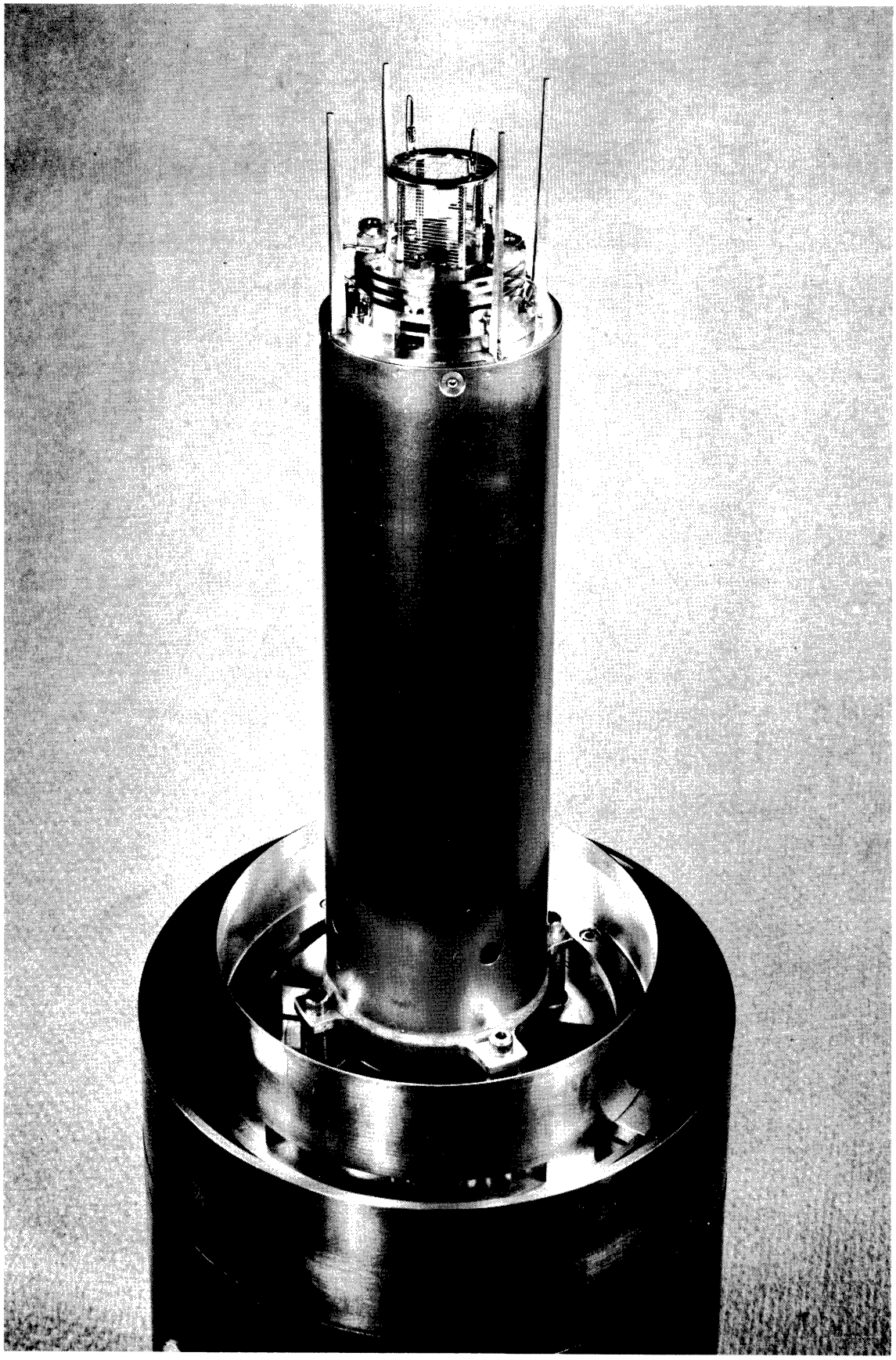

Figure 2. Flight model.

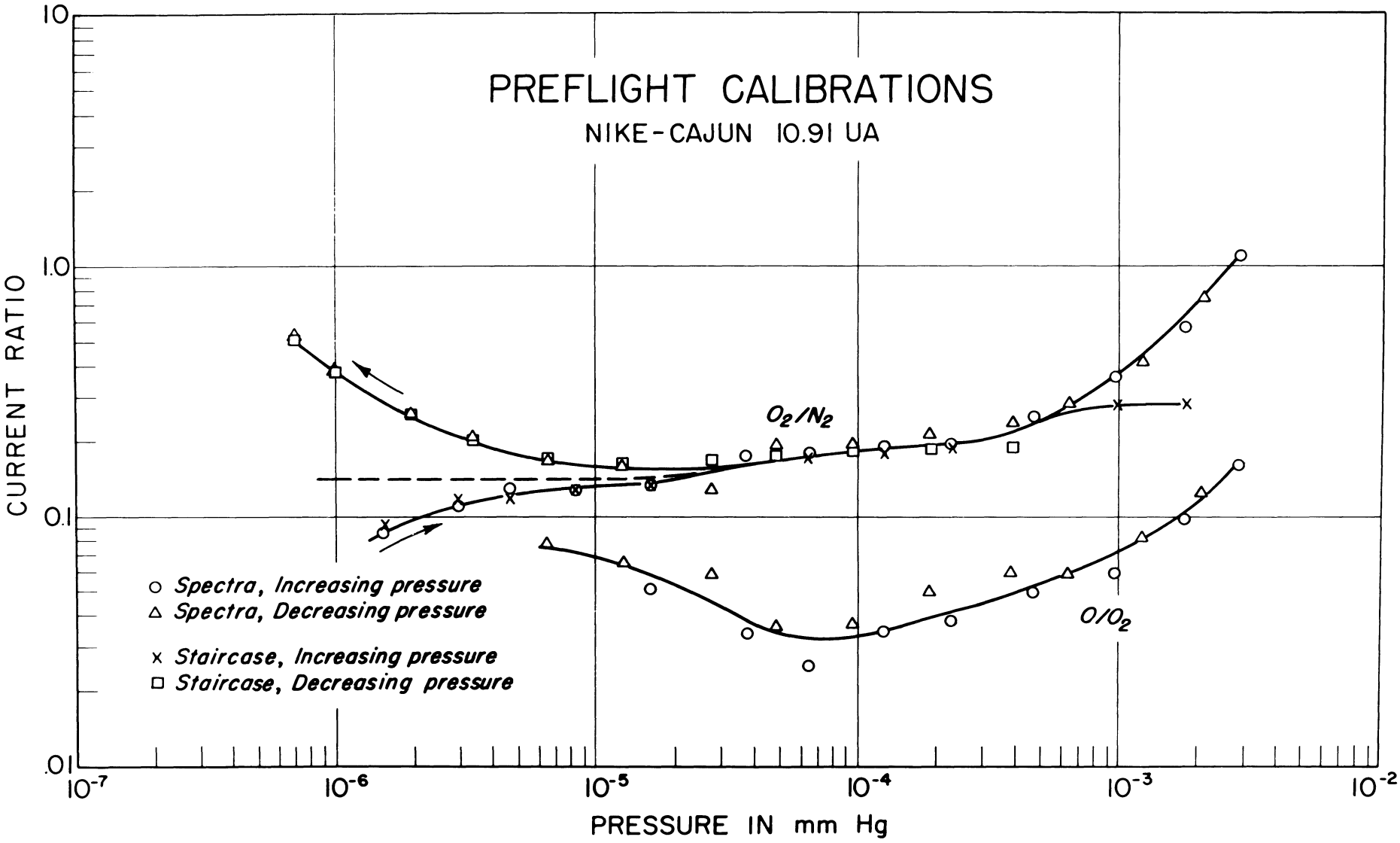

Figure 3. Preflight calibrations (O_2/N_2 and O_1/O_2).

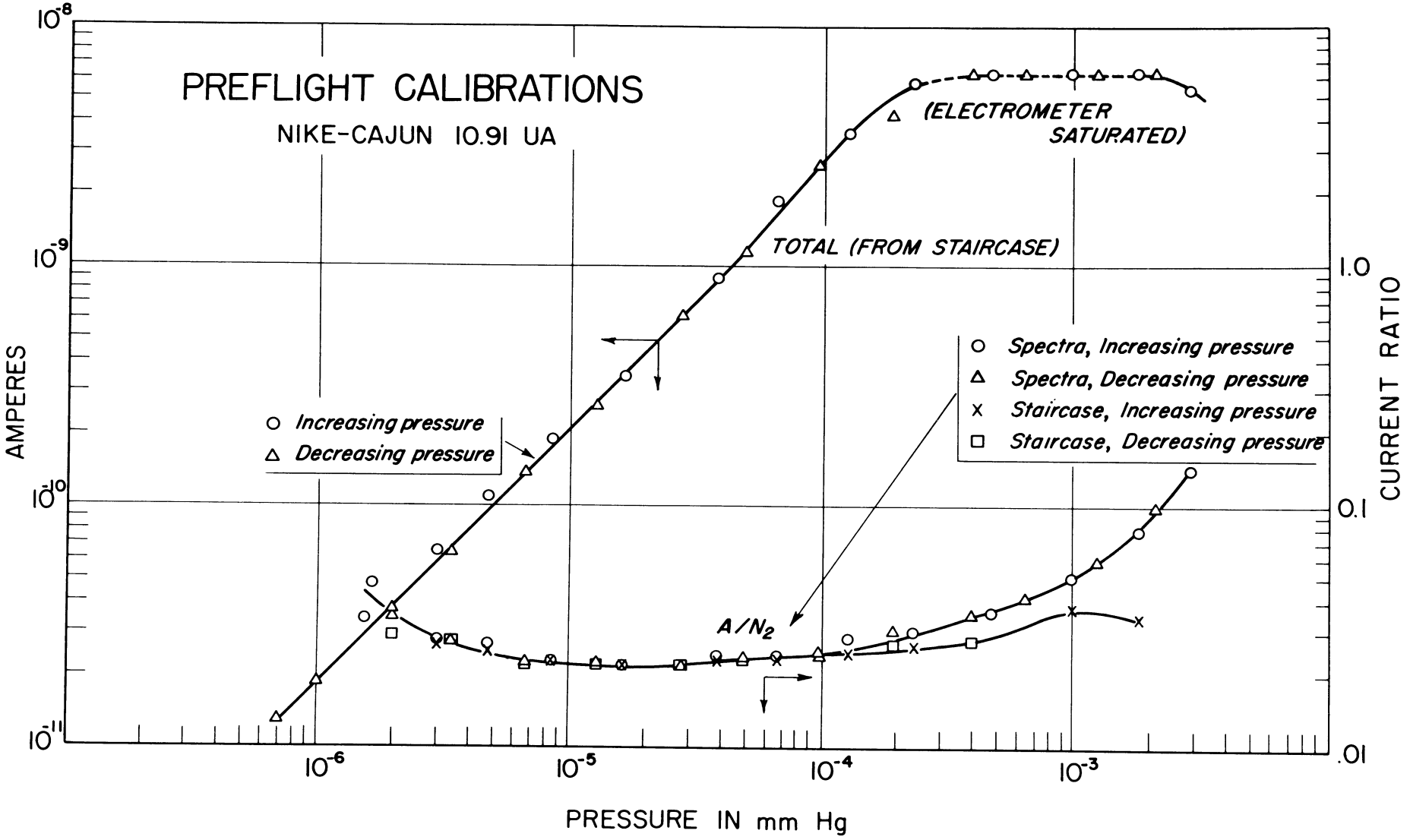

Figure 4. Preflight calibrations (total and A/N_2).

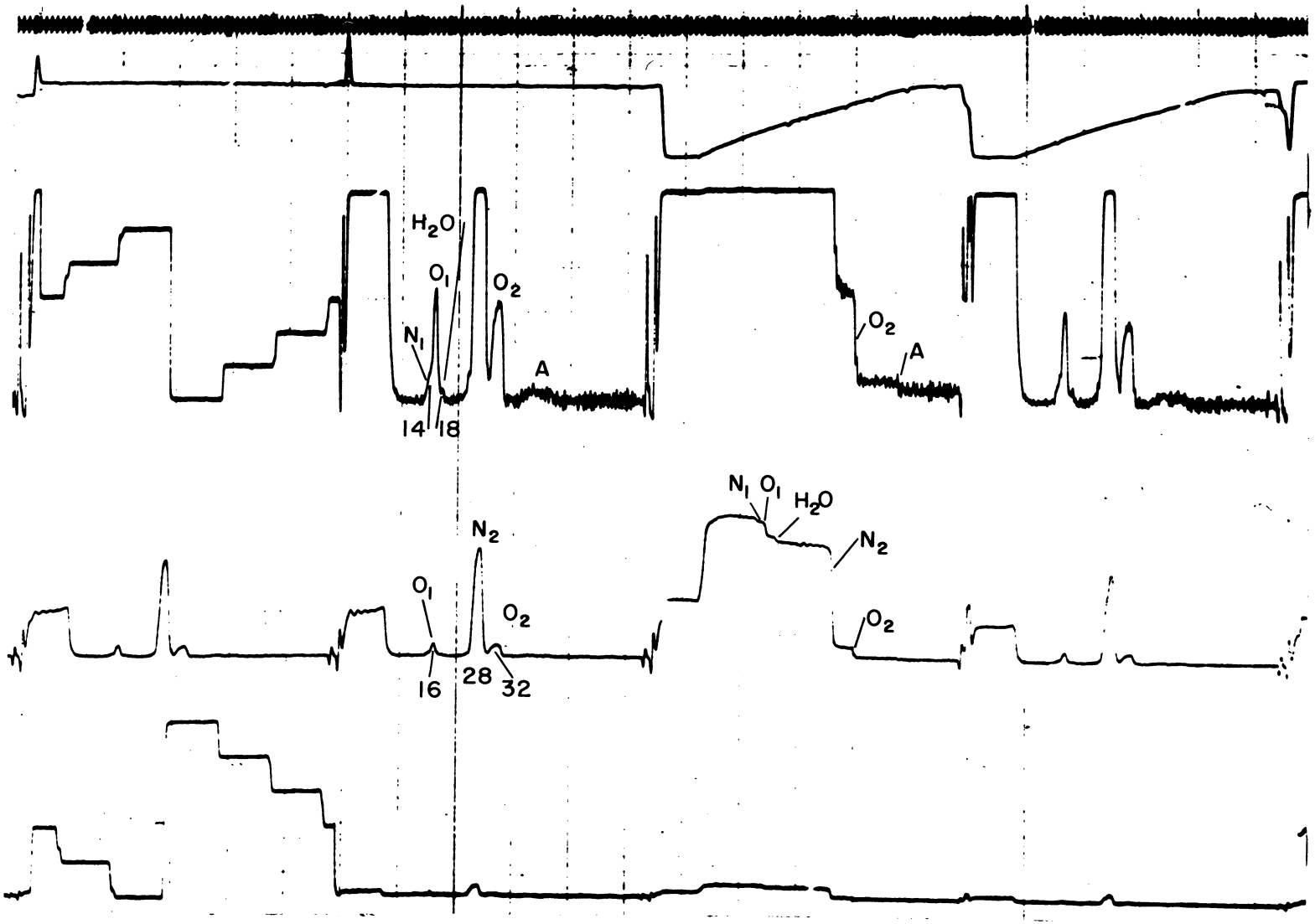

NIKE-CAJUN-1091 UA---120KM-UPLEG-124SEC

Figure 5. Flight spectra.

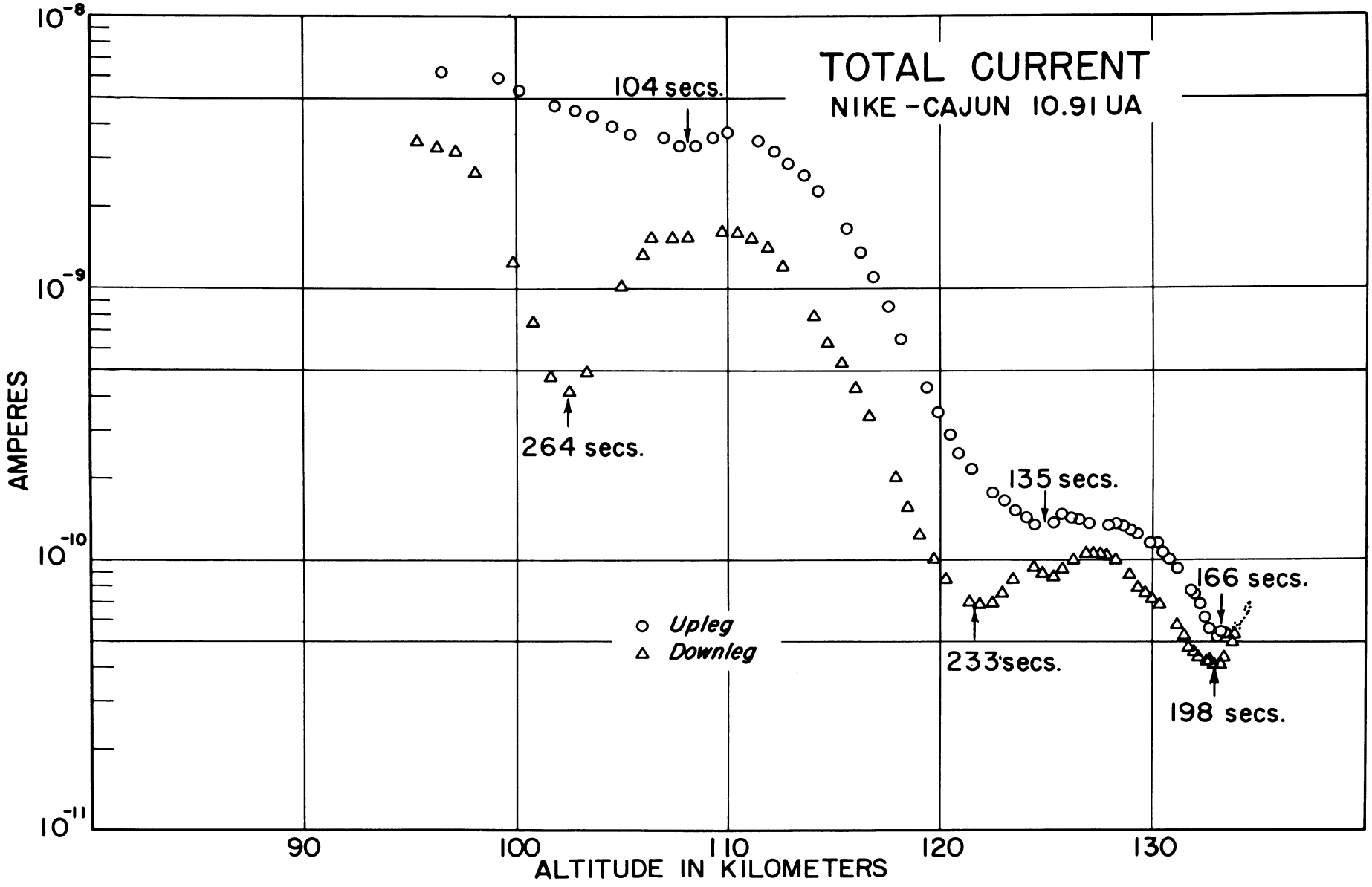

(a) Total current.

Figure 6. Flight raw data.

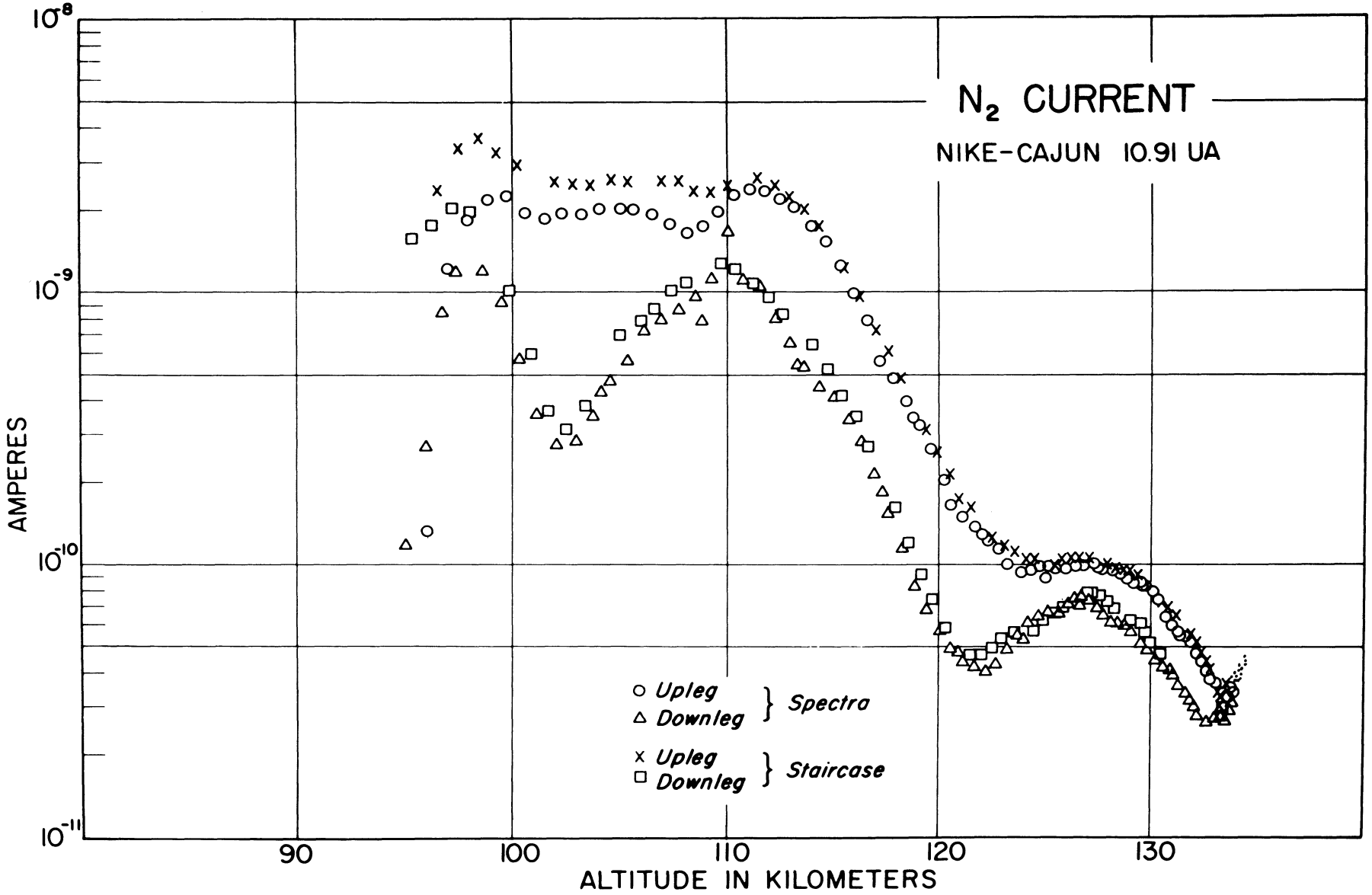

(b) N_2 current.

Figure 6. Continued.

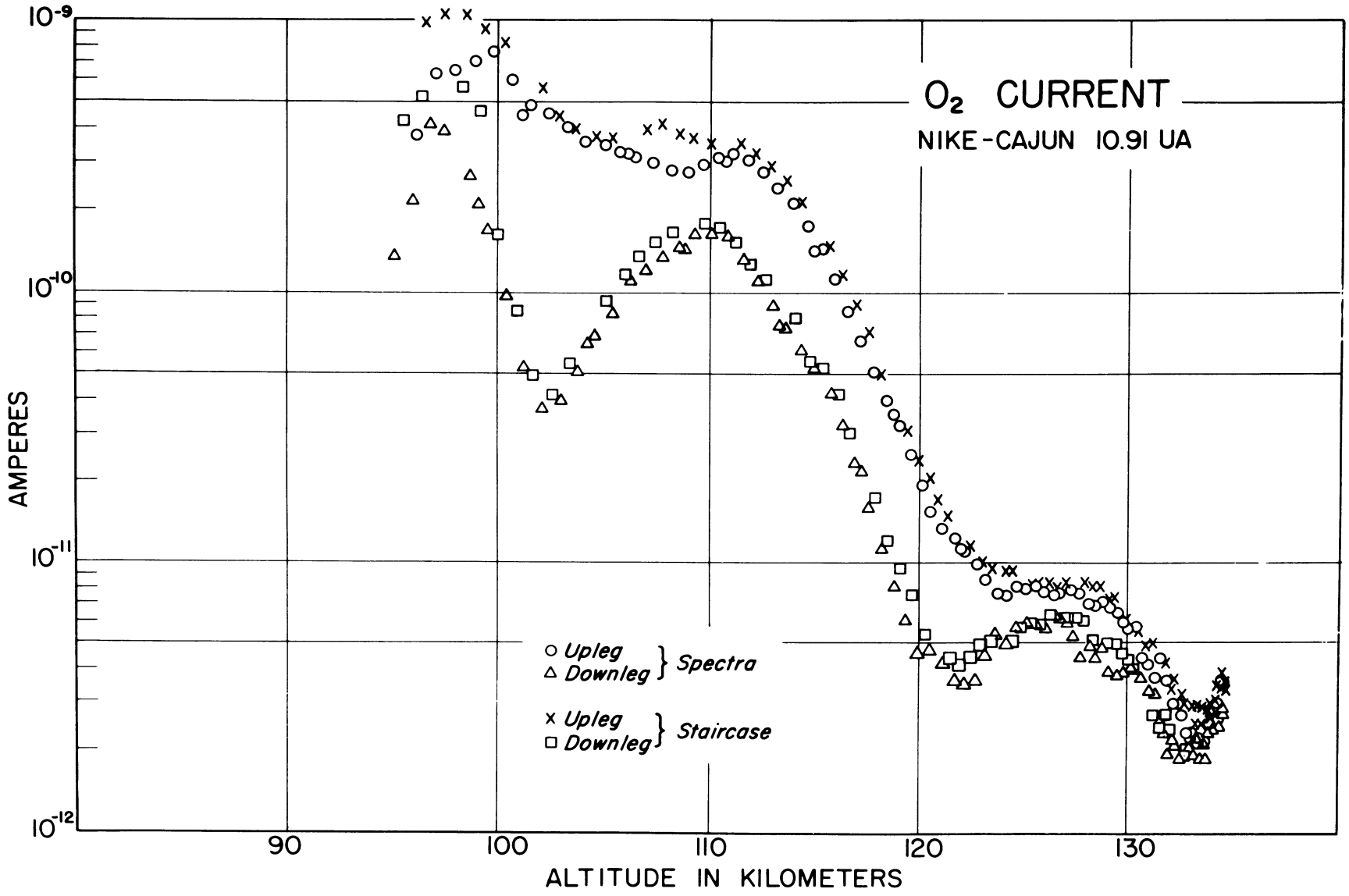

(c) O_2 current.

Figure 6. Continued.

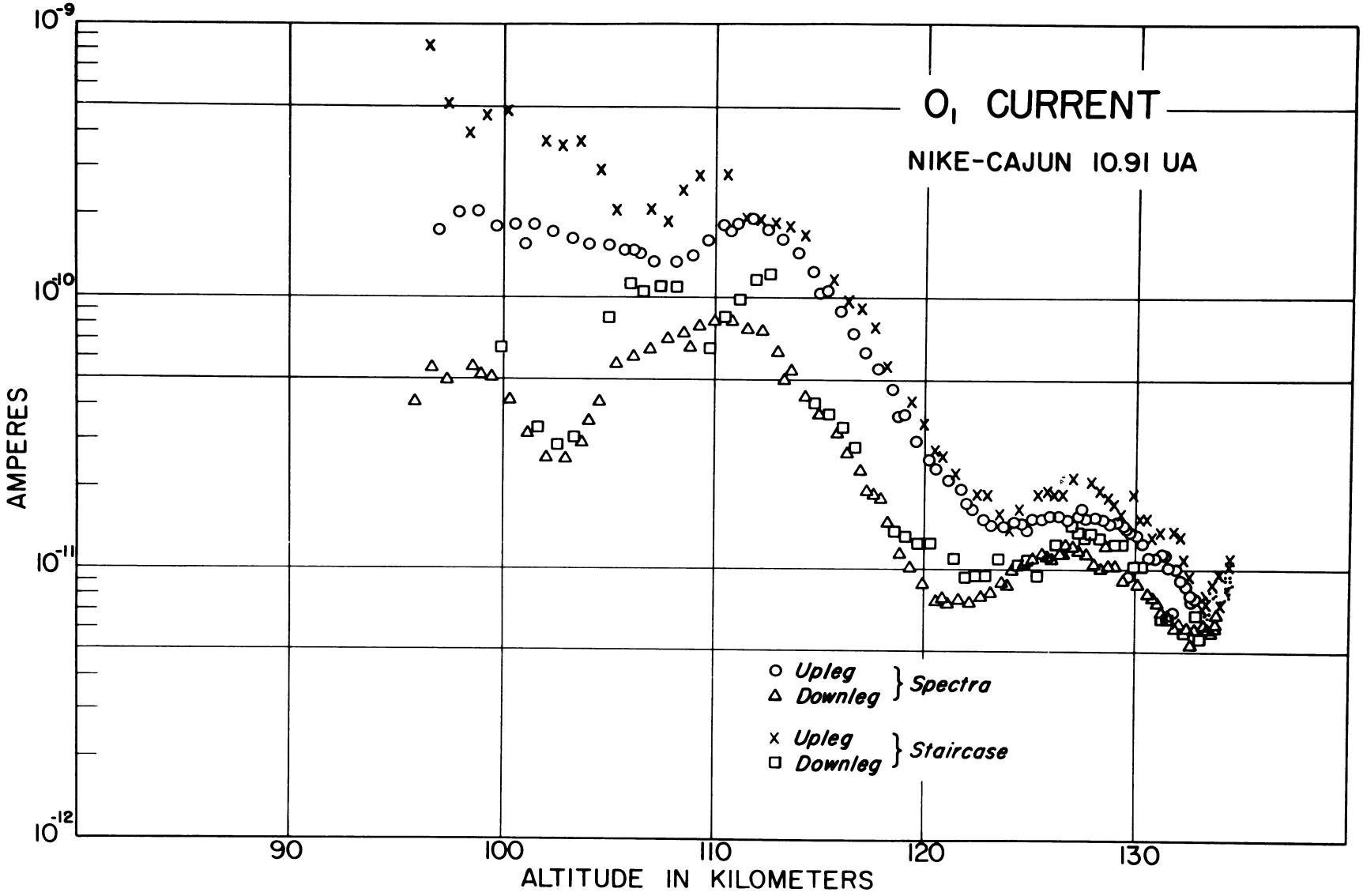

(d) O_1 current.

Figure 6. Continued.

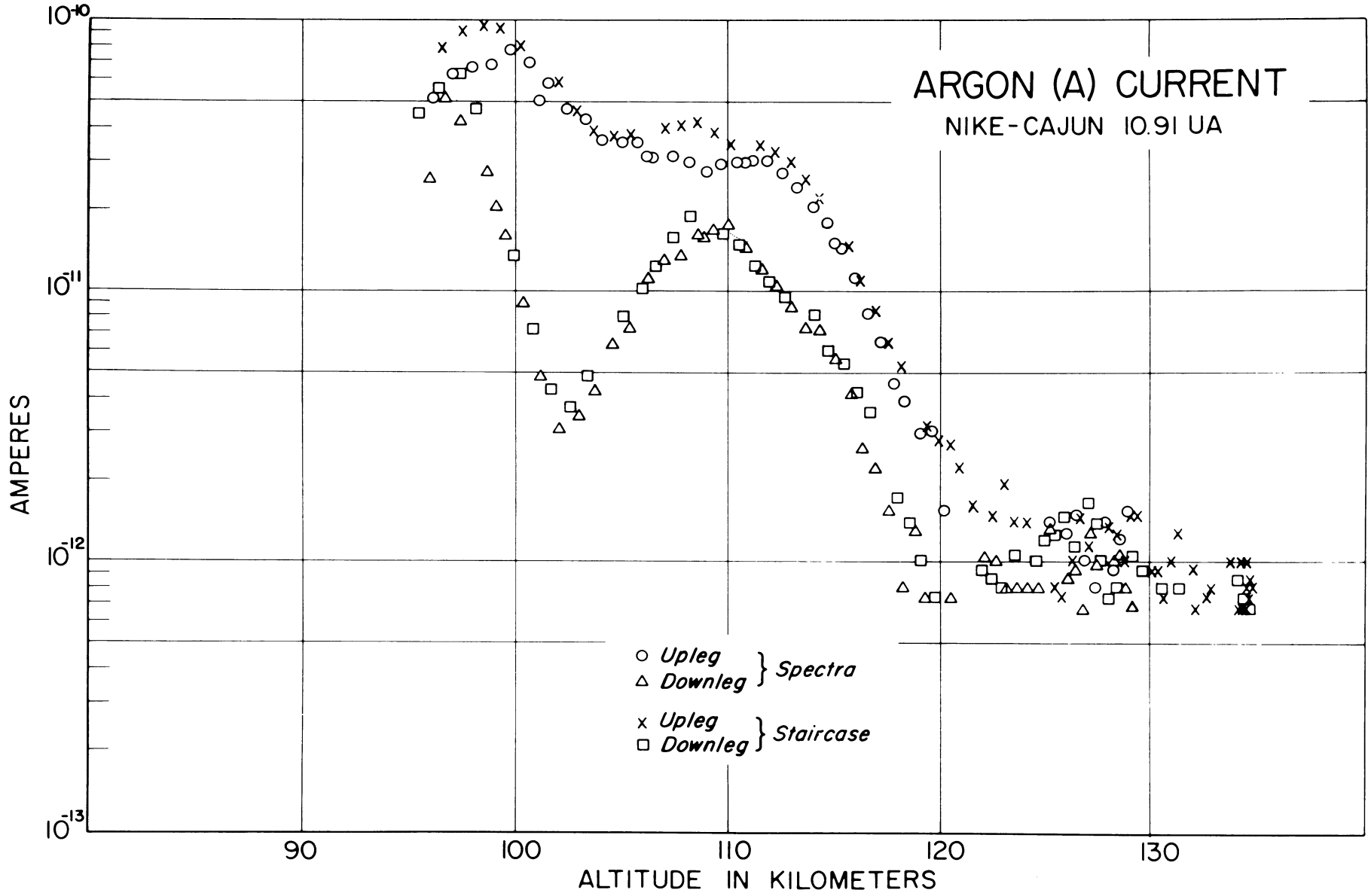

(e) Argon (A) current.

Figure 6. Concluded.

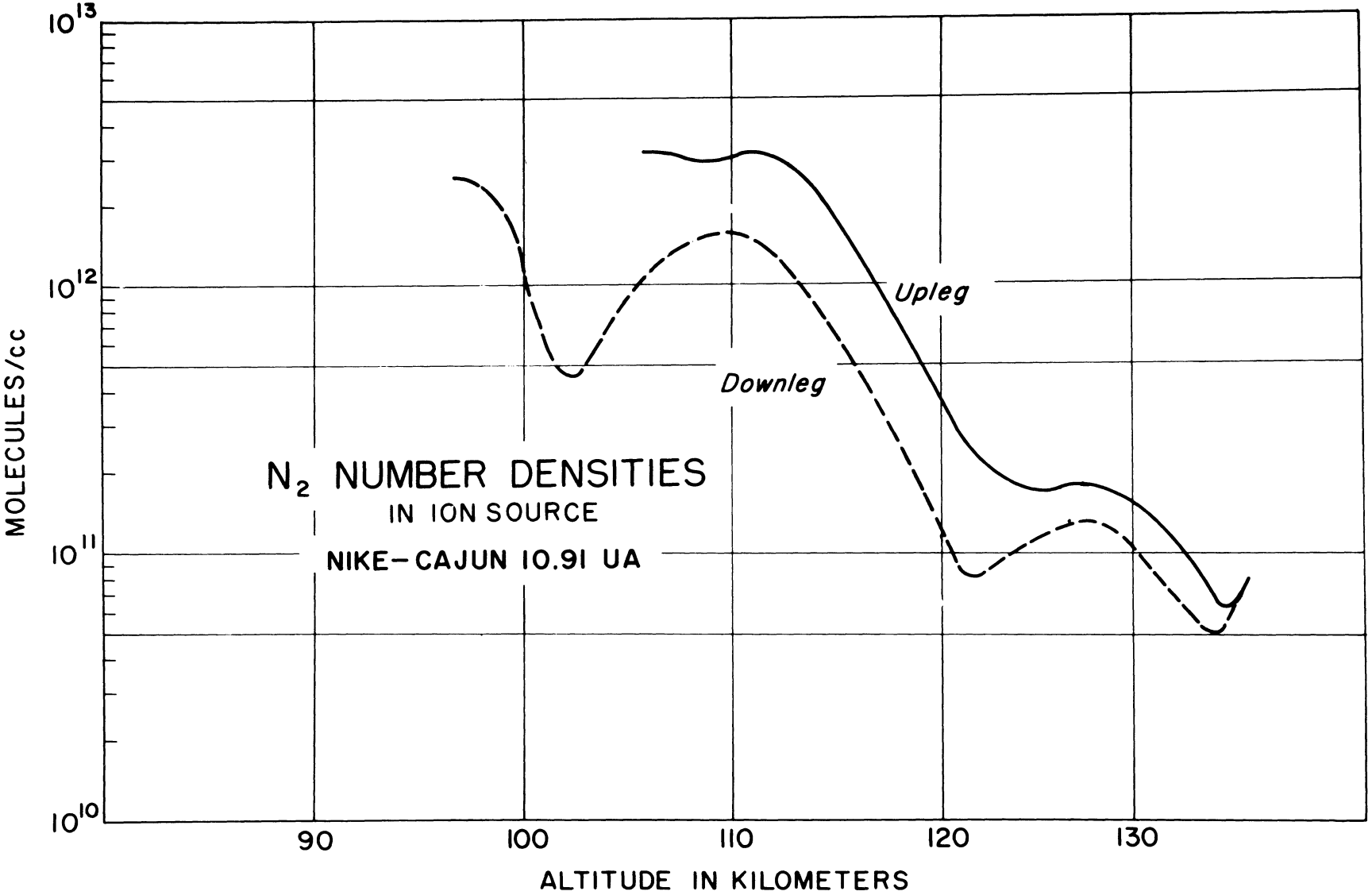

(a) N_2 number densities.

Figure 7. Computed concentrations.

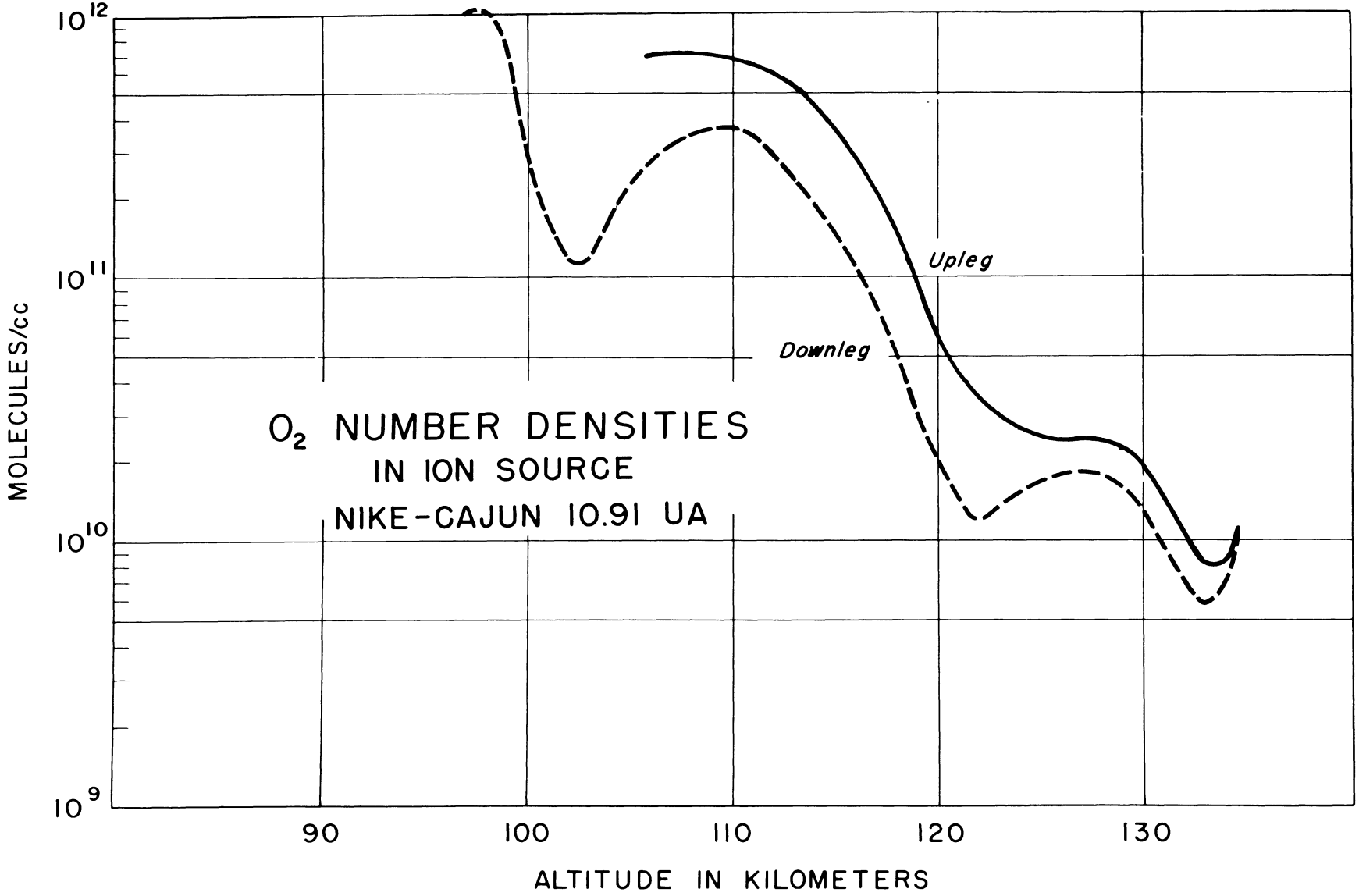

(b) O_2 number densities.

Figure 7. Continued.

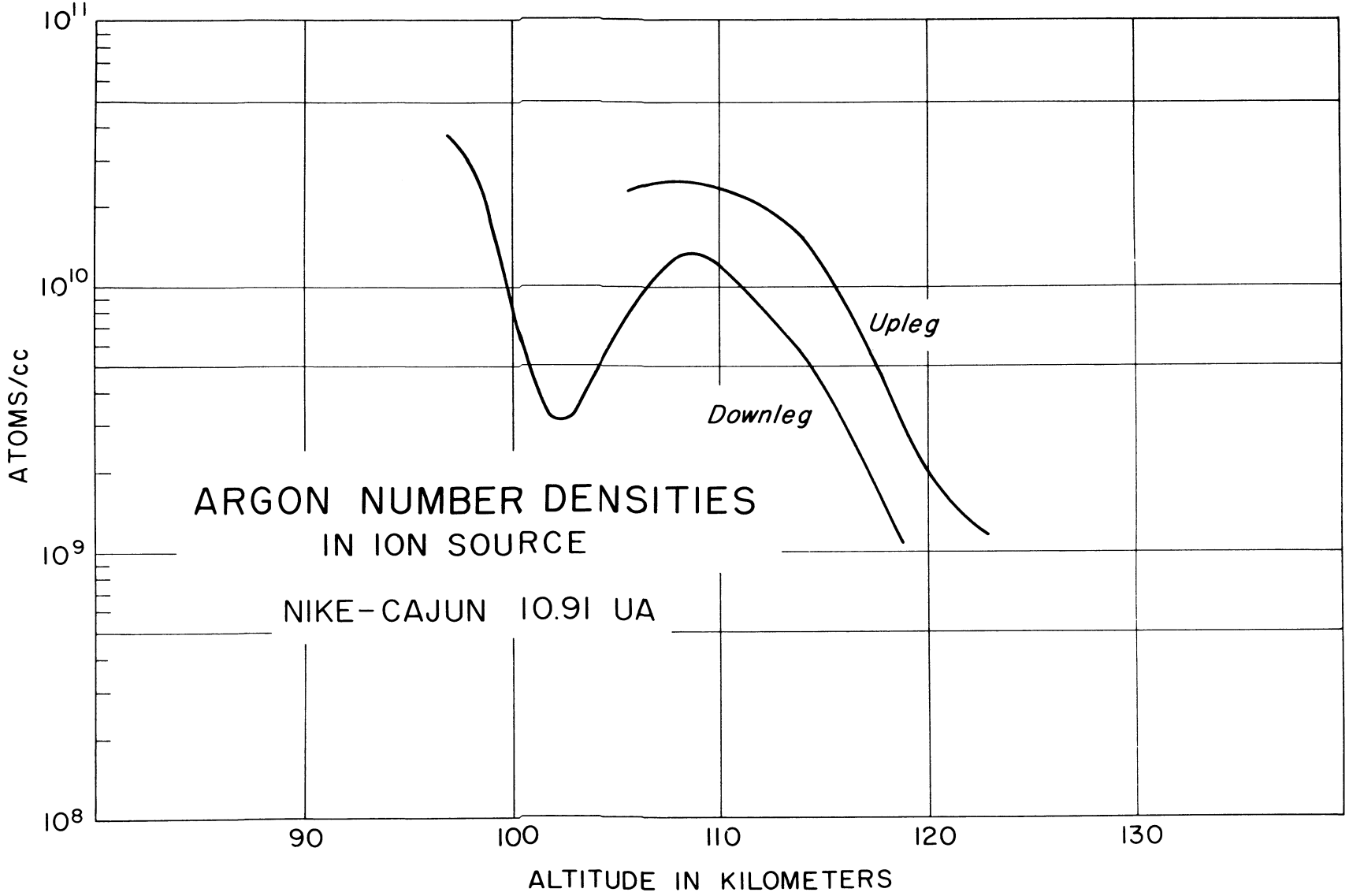

(c) Argon number densities.

Figure 7. Concluded.

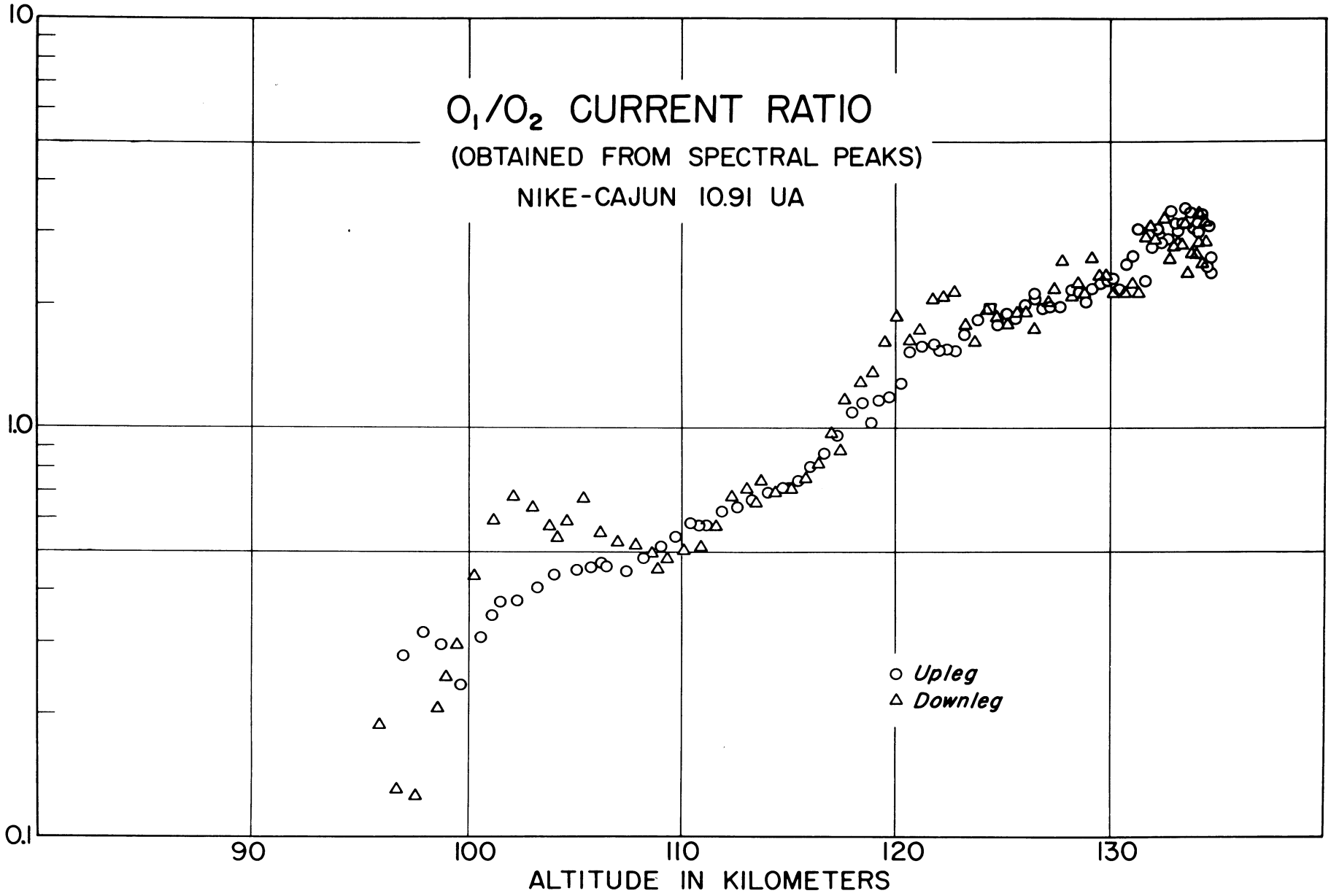

Figure 8. O_1/O_2 current ratio.

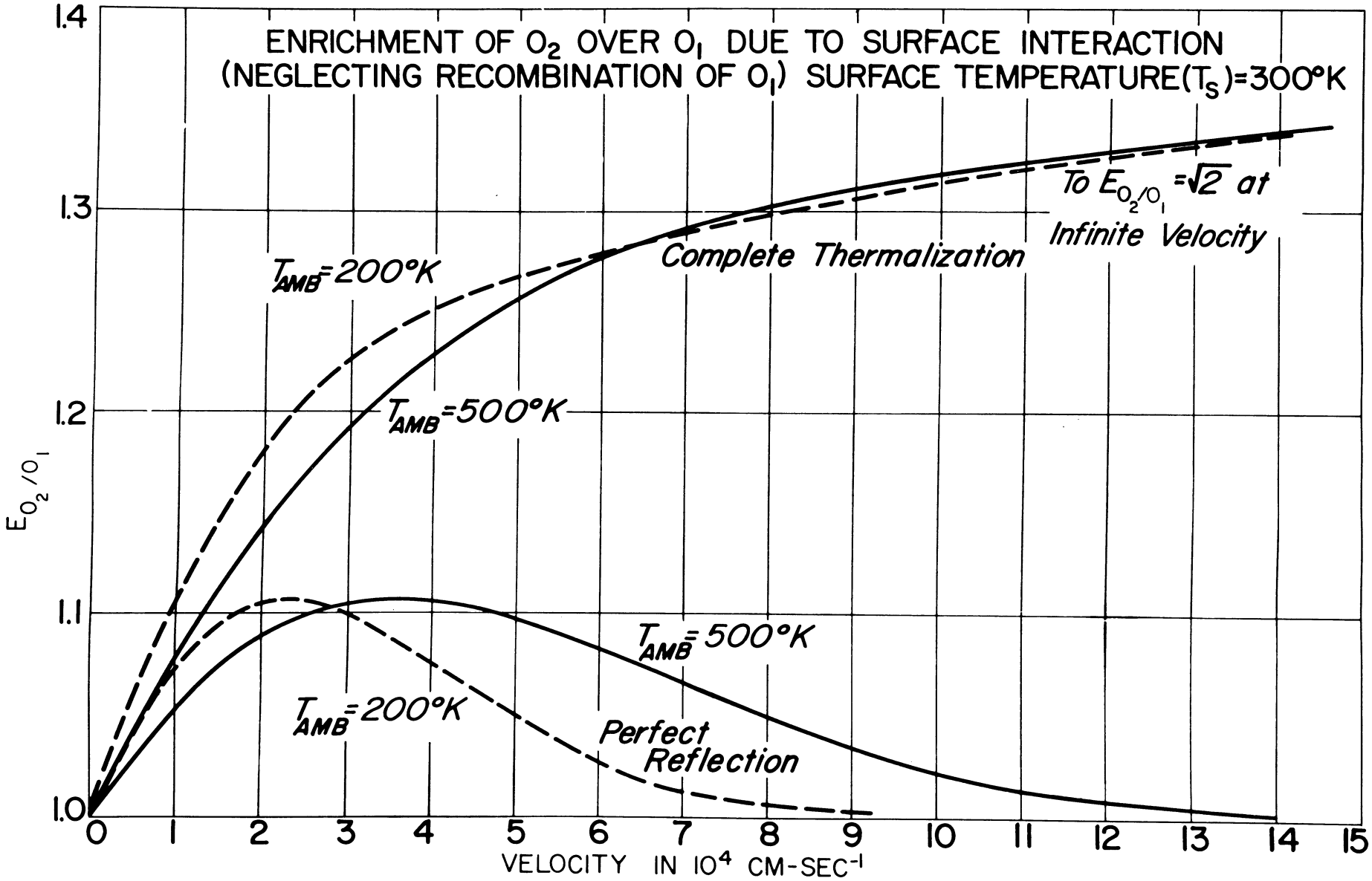

Figure 9. Enrichment factor of O_2 over O_1.

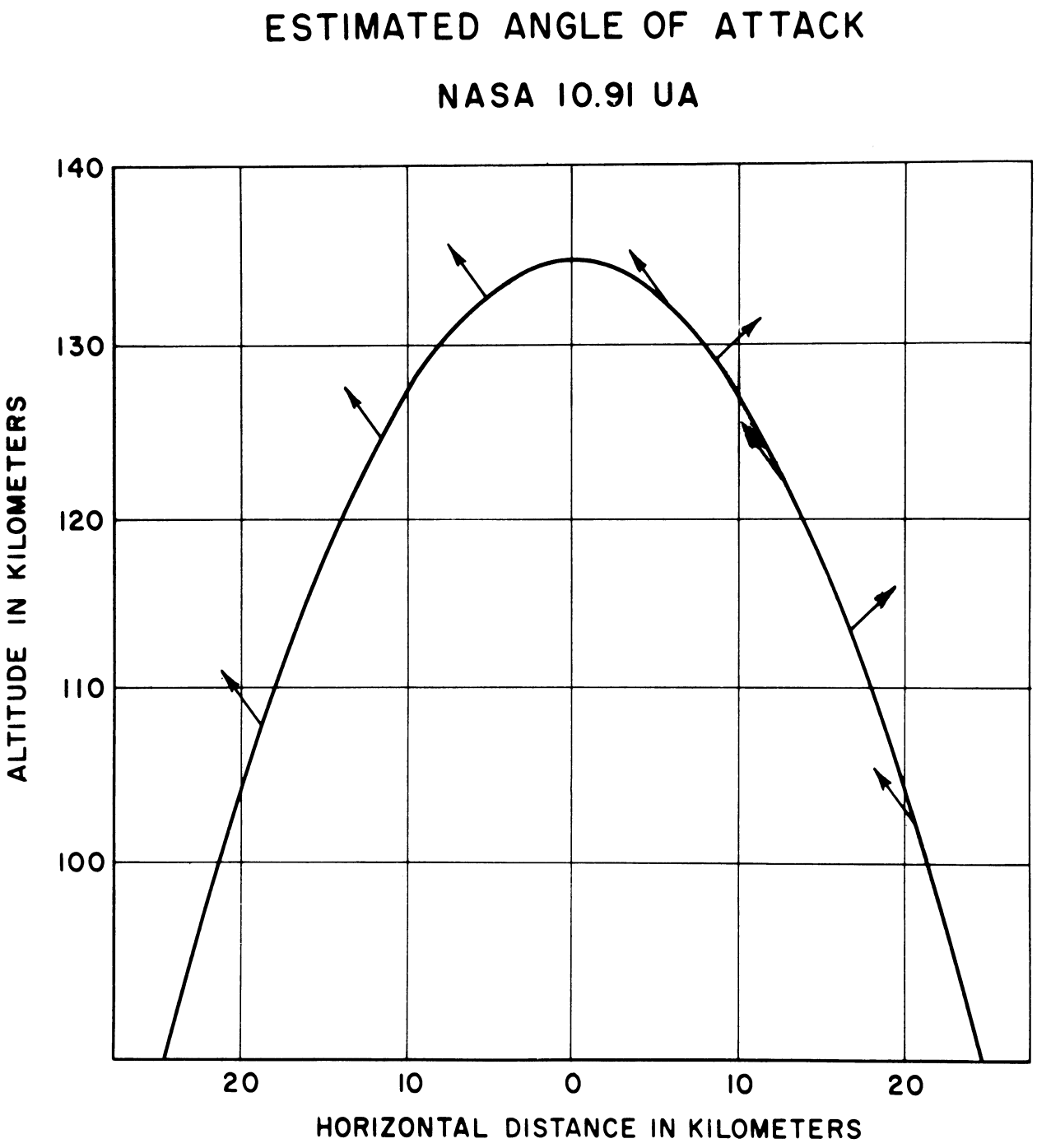

Figure 10. Estimated angle of attack.

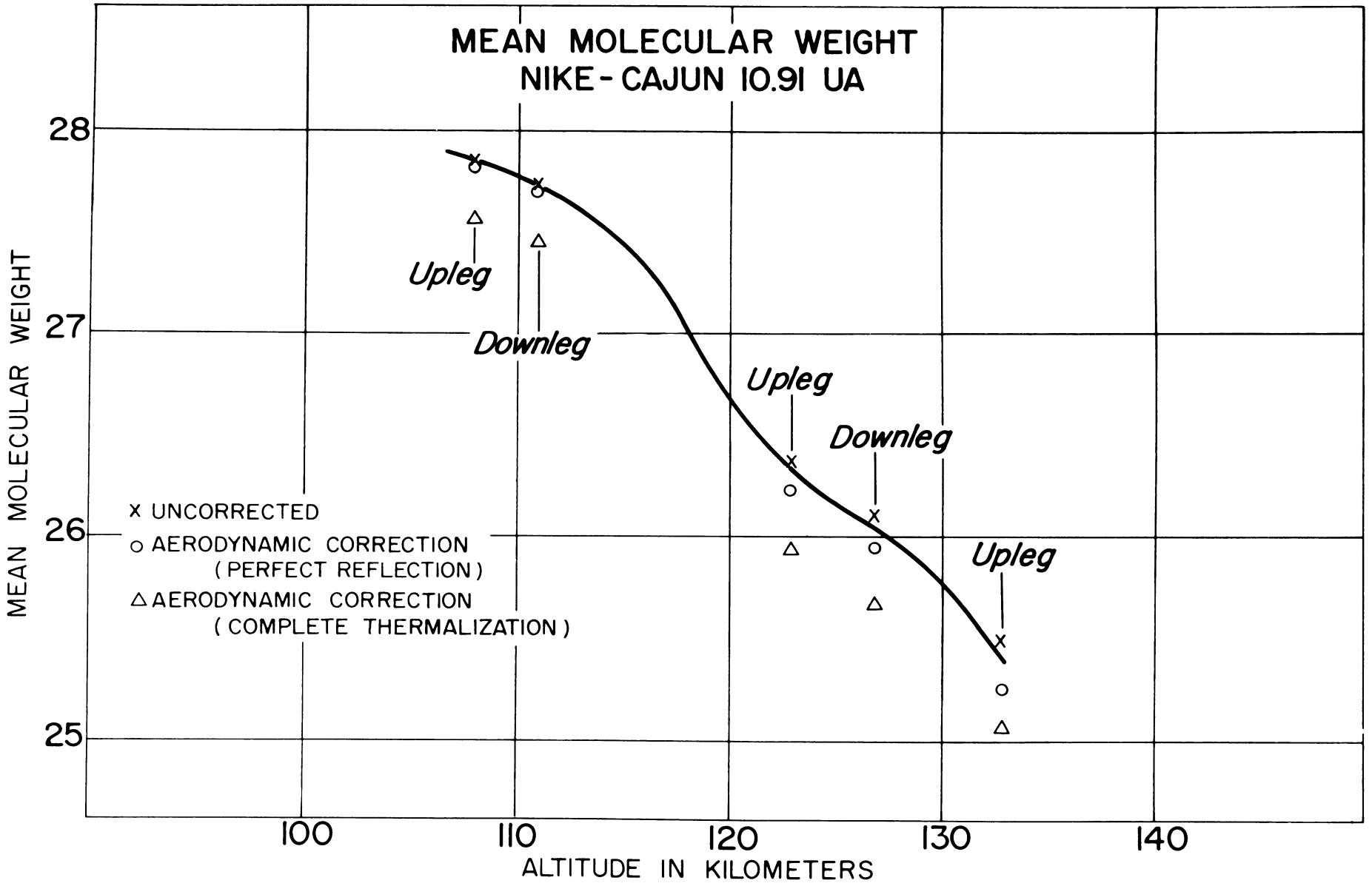

Figure 11. Mean molecular weight.

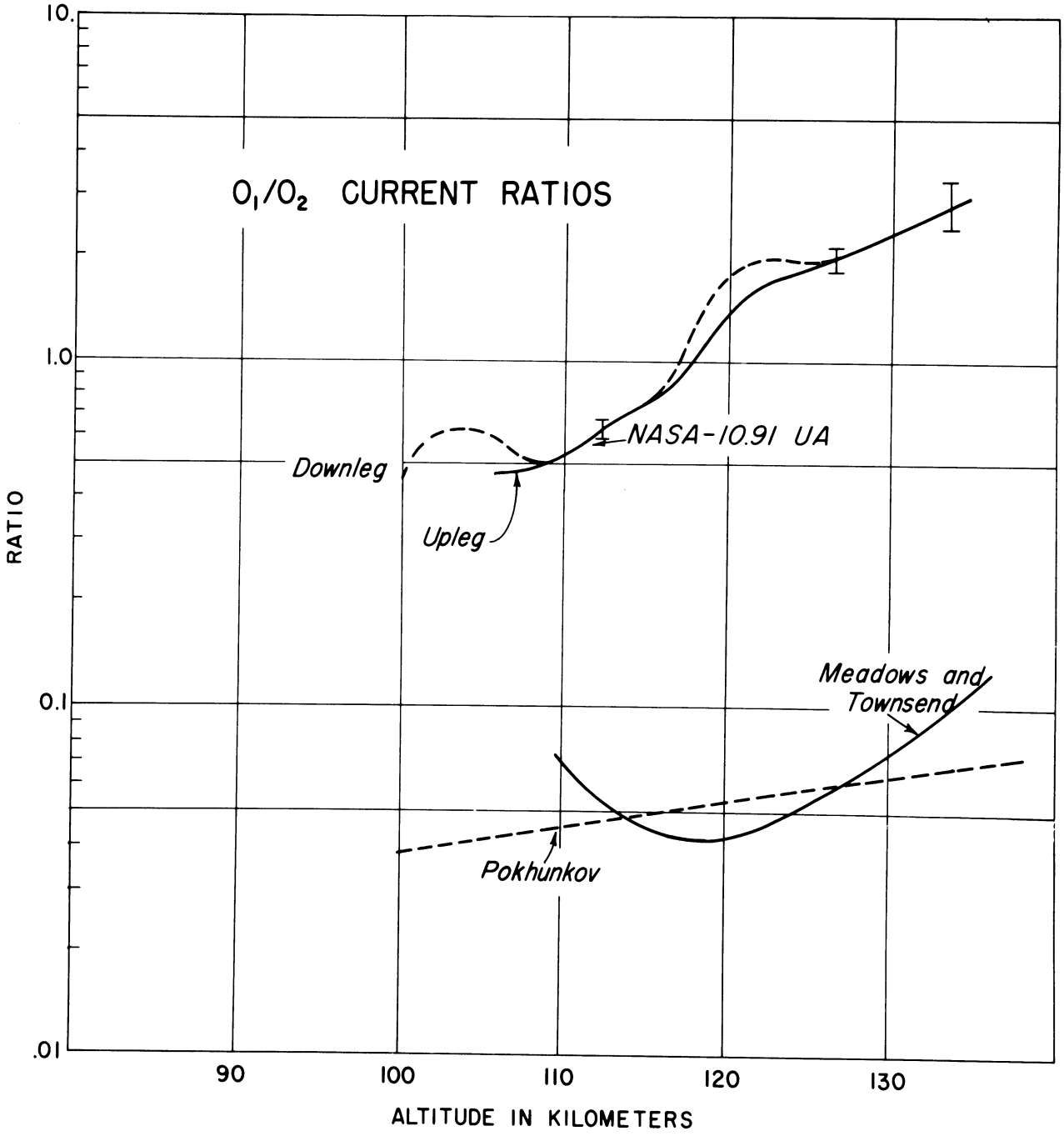

Figure 12. O_1/O_2 current ratios.

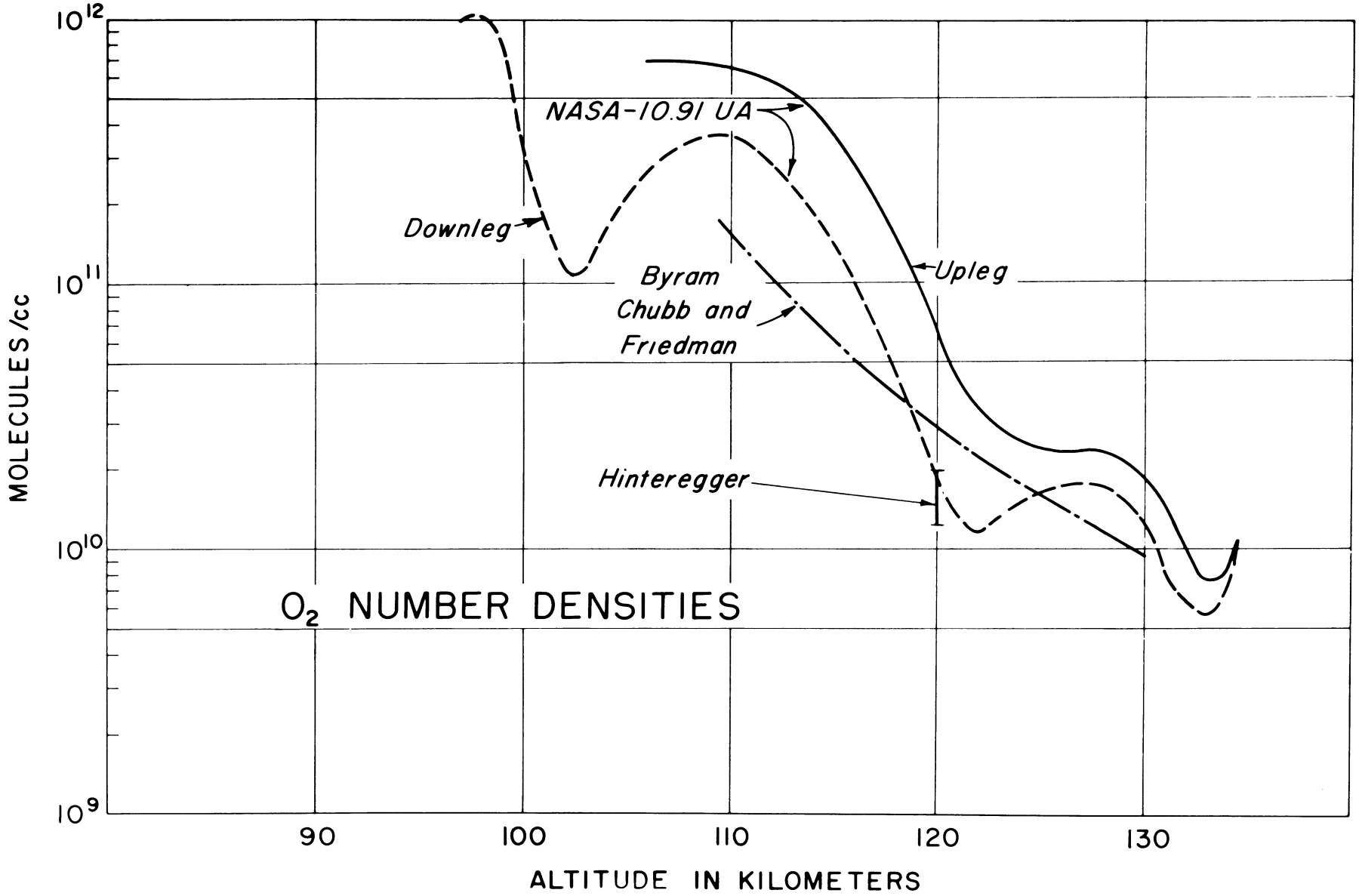

Figure 13. O_2 number densities.

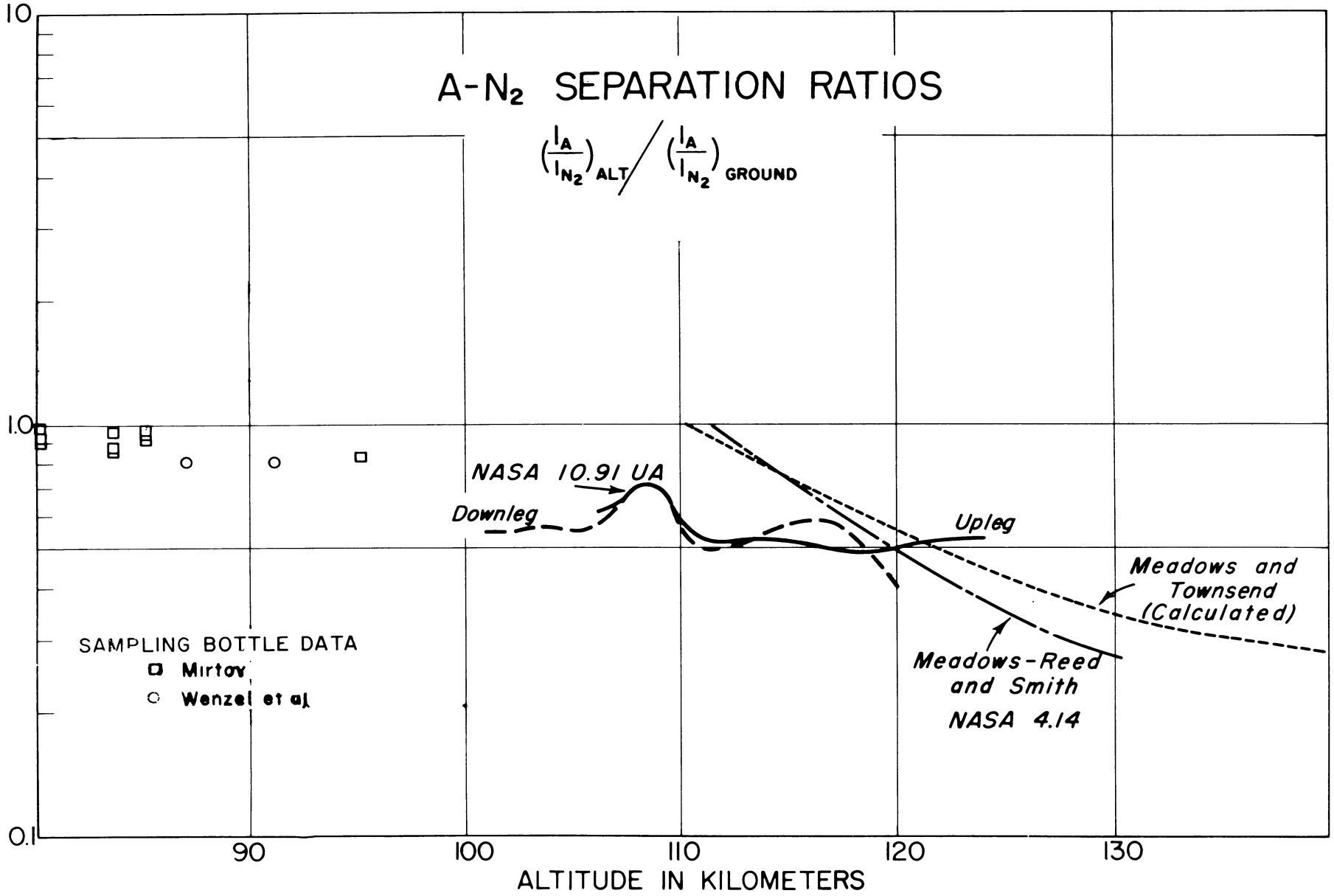

Figure 14. A/N_2 separation ratios.

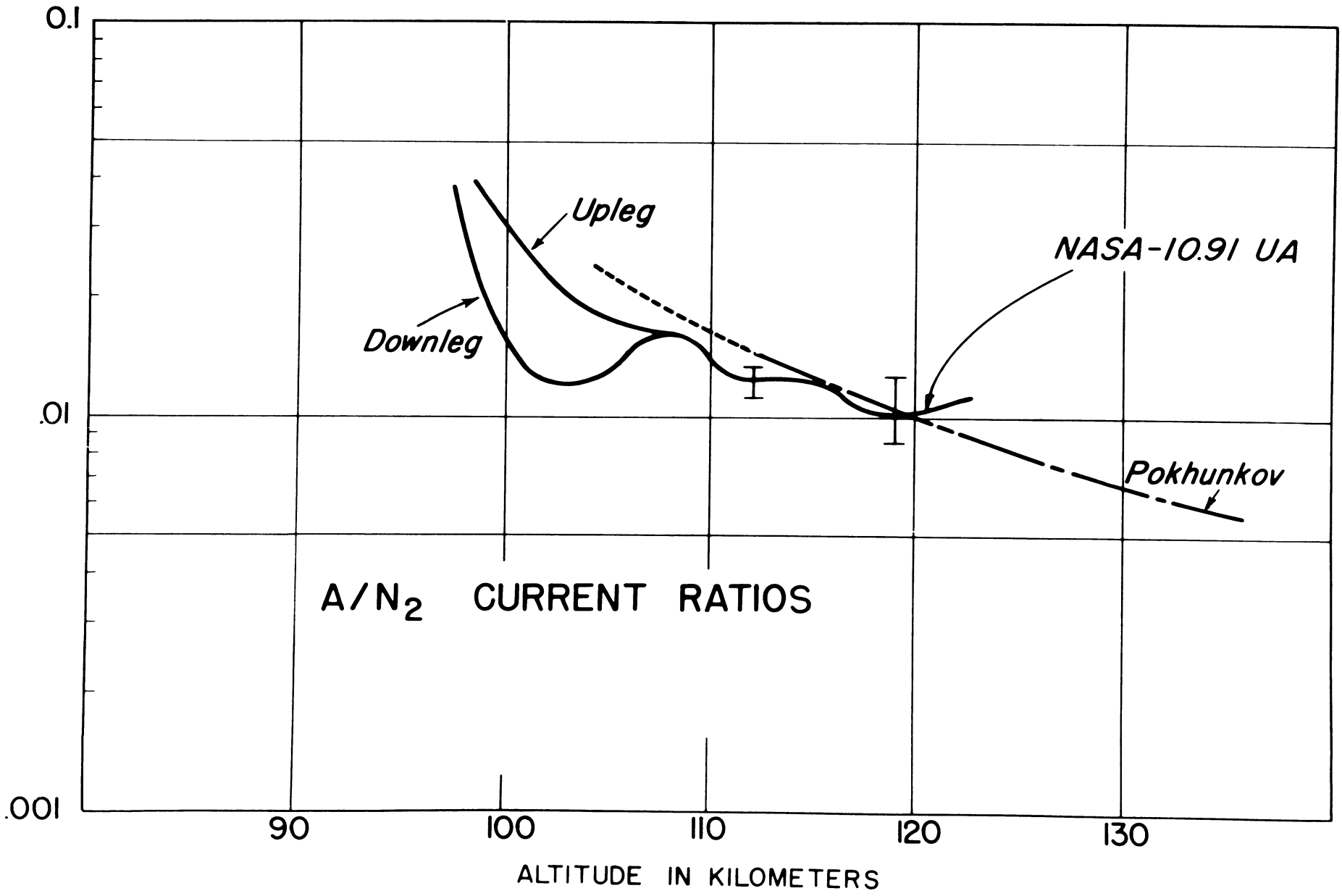

Figure 15. A/N_2 current ratios.

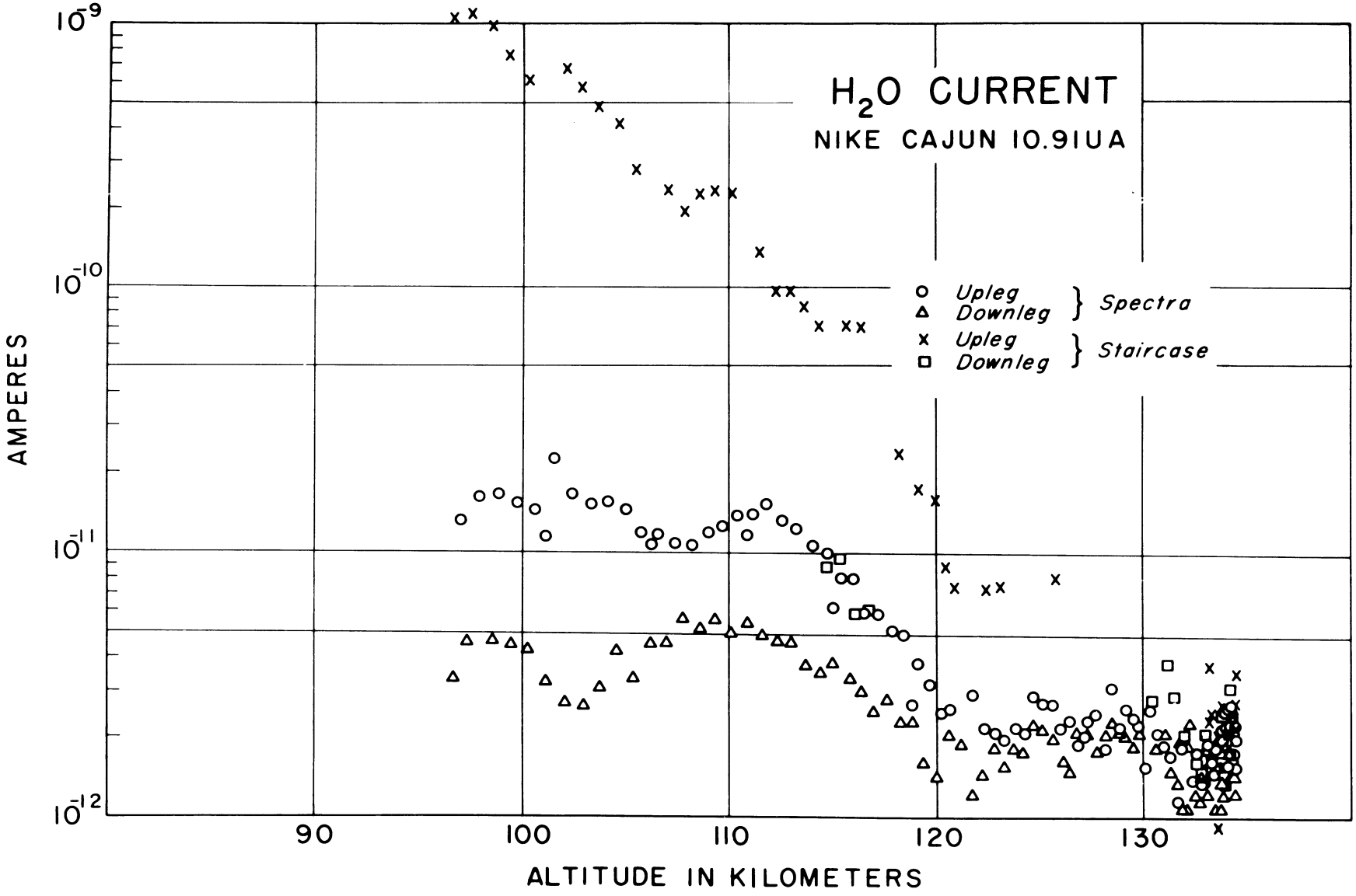

Figure 16. Flight raw data, H_2O current.

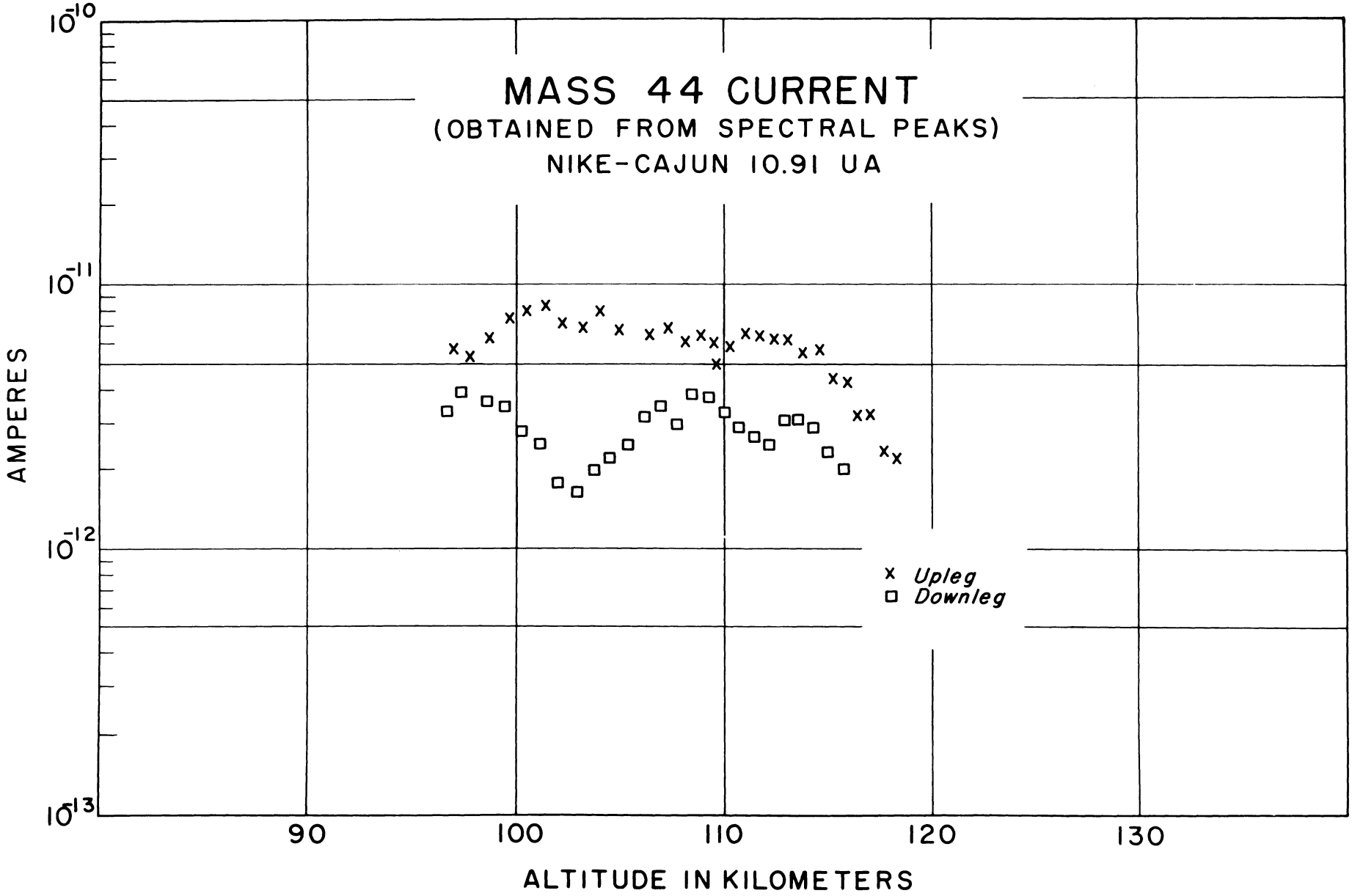

Figure 17. Flight raw data, mass 44 current.

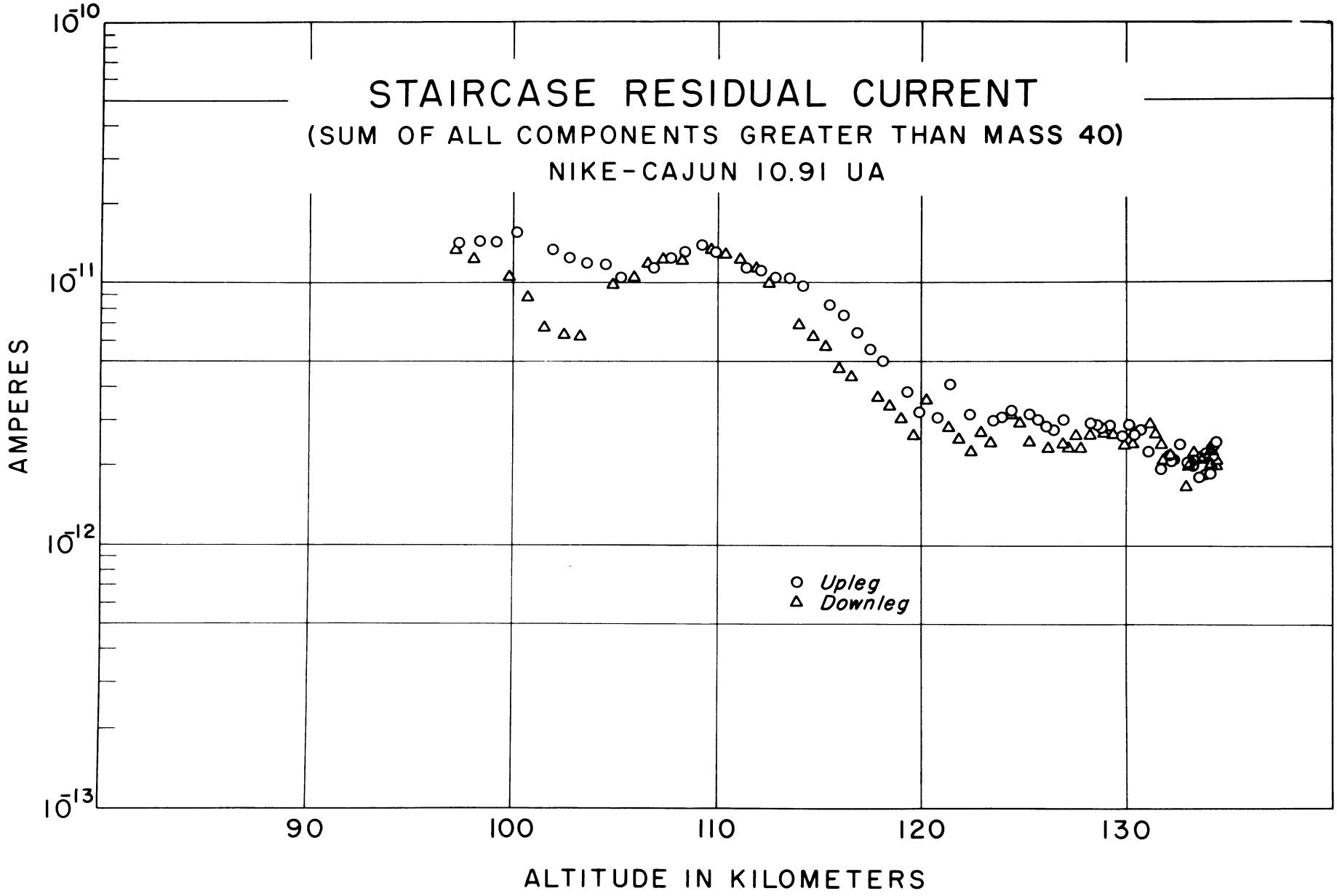

Figure 18. Flight raw data, staircase residual current.